UNIVERSITAS INDONESIA

Synthesis of Tungsten Oxide Thin Film and Nanowires for Highly Improved Electrochromic Smart Windows

TESIS

Nama: Tomy Abuzairi
NPM: 0906644120

FAKULTAS TEKNIK
PROGRAM STUDI TEKNIK ELEKTRO
DEPOK, JAWA BARAT
JANUARI 2012

UNIVERSITAS INDONESIA

Synthesis of Tungsten Oxide Thin Film and Nanowires for Highly Improved Electrochromic Smart Windows

TESIS

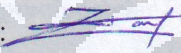Diajukan sebagai salah satu syarat untuk memperoleh gelar Magister Teknik

Nama: Tomy Abuzairi
NPM: 0906644120

FAKULTAS TEKNIK
PROGRAM STUDI TEKNIK ELEKTRO
DEPOK, JAWA BARAT
JANUARI 2012

HALAMAN PERNYATAAN ORISINALITAS

Tesis ini adalah hasil karya saya sendiri

dan semua sumber baik yang dikutip maupun dirujuk

telah saya nyatakan dengan benar

Nama   : Tomy Abuzairi

NPM   : 0906644120

Tanda Tangan   :

Tanggal   : 9 Januari 2012

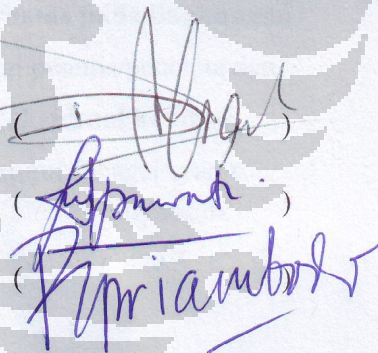# HALAMAN PENGESAHAN

Tesis ini diajukan oleh

Nama   : Tomy Abuzairi

NPM   : 0906644120

Program Studi   :Teknik Elektro

Judul tesis   : Synthesis of Tungsten Oxide Thin Film and Nanowires For Highly Improved Electrochromic Smart Windows

Telah berhasil dipertahankan di hadapan Dewan Penguji dan diterima sebagai bagian persyaratan yang diperlukan untuk memperoleh gelar Magister Teknik pada Program Studi Teknik Elektro, Fakultas Teknik, Universitas Indonesia.

DEWAN PENGUJI

Penguji   : Prof. Dr. Ir. Djoko Hartanto M.Sc.   (   )

Penguji   : Prof. Dr.Ir Nji Raden Poespawati M.T.   (   )

Penguji   : Ir. Purnomo Sidi Priambodo M.Sc., Ph.D.   (   )

Ditetapkan di   : Depok, Jawa Barat

Tanggal   : 9 Januari 2012

HALAMAN PERNYATAAN PERSETUJUAN PUBLIKASI
TUGAS AKHIR UNTUK KEPENTINGAN AKADEMIS

Sebagai sivitas akademik Universitas Indonesia, saya yang bertanda tangan di bawah ini:

Nama : Tomy Abuzairi

NPM : 0906644120

Departemen : Teknik Elektro
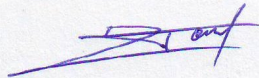
Fakultas : Teknik

Jenis karya : Tesis

demi pengembangan ilmu pengetahuan, menyetujui untuk memberikan kepada Universitas Indonesia **Hak Bebas Royalti Noneksklusif** (*Non-exclusive Royalty-Free Right*) atas karya ilmiah saya yang berjudul : Synthesis of Tungsten Oxide Thin Film and Nanowires For Highly Improved Electrochromic Smart Windows.

Dengan Hak Bebas Royalti Noneksklusif ini Universitas Indonesia berhak menyimpan, mengalih media/formatkan, mengelola dalam bentuk pangkalan data (*database*), merawat, dan memublikasikan tugas akhir saya **untuk akses terbatas pada lingkungan internal kampus** dengan tetap mencantumkan nama saya sebagai penulis/pencipta dan sebagai pemilik Hak Cipta. Adapun untuk **akses secara umum/ eksternal kampus dapat dilakukan setelah 5 tahun** semenjak karya imiah ini disetujui sebagai syarat memperoleh gelar magister teknik.

Demikian pernyataan ini saya buat dengan sebenarnya.

Depok, 9 Februari 2012

Yang menyatakan,

Tomy Abuzairi

碩士學位論文指導教授推薦書

Master's Thesis Recommendation Form

Department : Graduate Institute of Electro-Optical Engineering

Student's Name: TOMY ABUZAIRI

Thesis title: Synthesis of Tungsten Oxide Thin Film and Nanowires for Highly Improved Electrochromic Smart Windows

This is to certify that the thesis submitted by the student named above, has been written under my supervision. I hereby approve this thesis to be applied for examination.

Advisor:Bohr-Ran Huang

Co-advisor:

Advisor's Signature: _____

Date: __|o| / |1| / |9|___ (yyyy/mm/dd)

碩士學位考試委員會審定書

Qualification Form by Master's Degree Examination Committee

Department:Graduate Institute of Electro-Optical Engineering

Student's Name:TOMY ABUZAIRI

Thesis Title:

Synthesis of Tungsten Oxide Thin Film and Nanowires for Highly Improved Electrochromic Smart Windows

This is to certify that the dissertation submitted by the student named above, is qualified and approved by the Examination Committee.

Degree Examination Committee

Members' Signatures:

Advisor:

Program Director's Signature:

Department/Institute Chairman's Signature:

Date: _____ / __ / __ (yyyy/mm/dd)

Synthesis of Tungsten Oxide Thin Film and Nanowires for Highly Improved Electrochromic Smart Windows

Student: Tomy Abuzairi

Advisor: Bohr-Ran Huang (黃柏仁)

Abstract

Tungsten oxide, has many interesting optical, electrical, structural, and chemical properties, are an ideal choice material for electrochromic smart windows devices. In this study, tungsten oxide thin films were prepared by the thermal oxidization on Tungsten/ITO/glass substrates at different heat-treatment temperatures. The optimum heat-treatment temperature, corresponding to the maximum electrochromic performance, was achieved by 550 ^{o}C. X-ray diffraction (XRD) analysis indicates that a tetragonal WO_3 phase formed at temperatures below 550 ^{o}C and the phase transformed to monoclinic $W_{18}O_{49}$ after the temperature was raised to 650 ^{o}C. The electrical properties analysis confirmed that the highest electrical conductivity show the superior electrochromic performance, with the maximum coloration efficiency value of 60.4 cm^2/C. The tetragonal WO_3 films, with heat-treatment temperature 550 ^{o}C and 450 ^{o}C, exhibit good electrochromic properties such as a high diffusion coefficient (1.7×10^{-11} cm^2/s), fast electrochromic response time (coloration time 1.6 s, bleaching time 1.2 s), and high coloration efficiency (60.4 cm^2/C).

Furthermore, tungsten oxide nanowires were prepared on a tungsten film (W)/ITO-glass substrate at 500 ^{o}C for electrochromic devices using the heat-treatment

I

technique. The electrical properties analysis confirmed that the highest electrical conductivity achieve the superior electrochromic performance with the maximum coloration efficiency value. The tungsten oxide nanowires shows excellent electrochromic properties such as a higher diffusion coefficient (2×10^{-9} cm^2/s), faster electrochromic response time (coloration time 1.7 s, bleaching time 1.1 s), and higher coloration efficiency (67.41 cm^2/C) than other tungsten oxide films without nanowires. Therefore, the tungsten oxides nanowire prepared by heat-treatment technique, corresponding to the maximum electrochromic performance, would be further adopted in the commercial application of smart windows.

II

Acknowledgment

Alhamdulillah, all praises to Allah SWT who gives me ease in doing this thesis. This thesis also would not have been possible without the guidance and the help of several individuals who in one way or another contributed and extended their valuable assistance in the preparation and completion of this study.

First and foremost, my utmost gratitude to Prof. Bohr-Ran Huang (黃柏仁) as my research advisor in Taiwan Tech whose sincerity and encouragement I will never forget. I would also like to extend my appreciation to my advisors in UI-Indonesia: Prof. Djoko Hartanto, Prof. N.R. Poespawati, and Dr. Purnomo Sidi Priambodo for their advices during my research.

I would also like to extend my deepest gratitude to my mother, my father, and my big family, thank you for your spiritual support.

Taiwan government scholarship for their scholarship support, without this support, I would not have a chance to be at National Taiwan University of Science and Technology (Taiwan Tech. University).

Special thanks to Dr. Tzu-Ching Lin, Yin-Kan Yang, and Jun-Cheng Lin for their assistance in the laboratory experiment. Also my lab mates, K.T. Chu, Max, Fantasy, Weber, Ahan, Jimmy, R.U. Ready, Ivy, and Jean, who assisted me during the experiment.
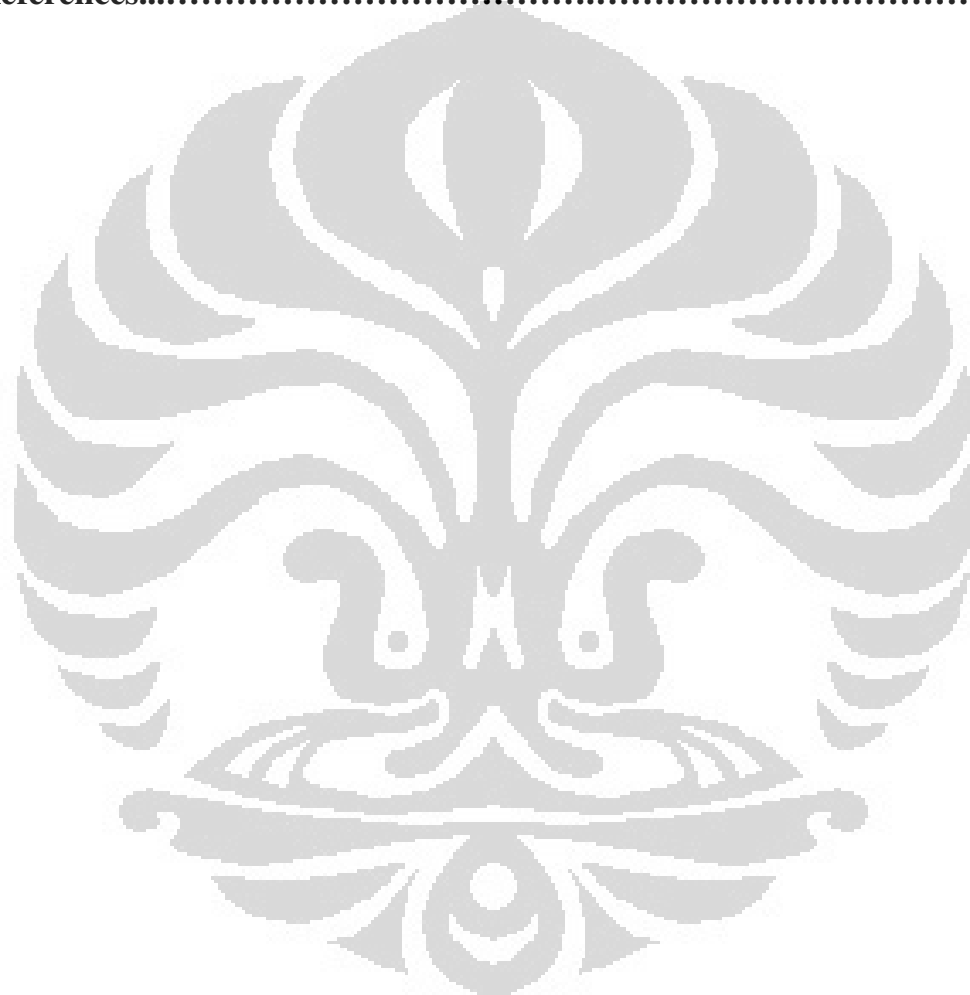
Last but not the least, administration officer of Taiwan Tech and UI-Indonesia who helped me in giving information, registration, and administration.

Contents

V

VI

List of Figures

IX

x

List of Tables

Chapter 1

Introduction

1.1 Background

Tungsten is a transition metal, along with molybdenum, iridium, and nickel, found in Group VI of the Periodic Table of elements. At the same time, tungsten oxide, which is one of the transition metal oxides, has many interesting optical, electrical, structural, and chemical properties. Those interesting properties make it suitable for various technological applications such as catalysts [1], gas sensors [2], field emitters [3], or electrochromic devices [4-6].

Among the numerous transition metal oxides, tungsten oxide are an ideal choice material for electrochromic devices and has been investigated in several books [7-8] and review articles [9-10]. Other metal oxides of lesser colorability are therefore more useful as optically passive, or nearly passive, counter electrodes [8].

In fact, there are four different fields within which electrochromic devices offer distinct advantages over alternative technologies [11]. From four different fields, smart windows attract more attention because of their proficiency in energy saving and comfortable indoor environment [12-13].

1

Modern man normally spends some 90% of his time inside buildings and vehicles, and the quality of the indoor environment hence is of the greatest importance. More and more energy is used to maintain the indoor environment at a level that is both comfortable and healthy. Looking at the EU, some 40% of the energy supply is used for heating, cooling, ventilation, and lighting of buildings, as well as for appliances; in financial terms this corresponds to about 4% of the gross national product. Another example is a recent study from Kuwait stating that more than 75% of the electricity is now consumed by air conditioning at peak load. When using "smart windows" instead of conventional static solar control windows, the energy for space cooling, on an annual basis, could be reduced by as much as 40–50% [14].

1.2 Motivation and aims

The motivation and aims of this study is mainly classified into two topics as follows:

1st topic: Effect of Heat-Treatment on the Properties of Tungsten Oxide Thermally Oxidized Films for Electrochromic Smart Windows

Tungsten oxide films for material of electrochromic smart windows have been grown by various methods, including sol-gel [15], spray pyrolysis [16], electrodeposition

2

[17], sputtering [18], electron beam evaporation [19], pulsed laser ablation [20], and thermal oxidization [21]. We opted for thermal oxidization process to prepare tungsten oxide film since it was, in comparison to thin film methods techniques, technically simple. In addition, the growing of tungsten oxide thin film on a supporting substrate (ITO-glass substrate) for smart windows is challenging yet essential for tuning the electrochromic performance.

Many recent studies of tungsten oxide for smart window application have focused on growth, structural, and electrochromic properties [22-26]. However, there are a few reports on the electrical properties of the tungsten oxide film and their influence on electrochromic performance. In this work, a thermal oxidization process was employed to synthesis tungsten oxide on ITO-glass substrates for smart windows. Furthermore, the structural, electrical, and electrochromic properties of tungsten oxide films have been investigated at different substrate temperatures.

2nd topic: Tungsten Oxide Nanowires for Highly Improved Electrochromic Smart Windows

The electrochromic smart windows performance of tungsten oxide, such as coloration efficiency and response time, depends on its structure. Moreover, One-dimensional (1D) nanostructures with high surface-to-volume ratio and small

3

grain size have attracted extensive research interests. Nanostructure could enhance the electrochromic performances of tungsten oxide thin film [27-29]. Recently, the growth method of tungsten oxide nanowires has been reported by many research groups [30-36]. We opted for thermal oxidization process to prepare tungsten oxide nanowires since it was technically simple.

Our group has successfully synthesized tungsten oxide nanowires using sputtered films as tungsten material on Si Substrate [37], with advantageous technique of catalyst-free and low temperature growth on sputtered W film. Sputtered films are favorable for the fabrication of device containing nanowires, and this method is capable of pattern growth. Since the growth of tungsten oxide nanowires on a sputtered W Film/ITO-glass substrate is very difficult from direct oxidization, here a simple thermal oxidization using heat-treatment technique was proposed to grow tungsten oxide nanowires for electrochromic smart windows. However, many recent studies of tungsten oxide nanowires for electrochromic devices have focused on growth, structural, and electrochromic properties [22-26]. There are a few reports on the electrical properties and their influence on electrochromic performance. In this study, we investigated not only structural, optical, and electrochromic properties but also electrical properties and their influence on electrochromic performance of tungsten oxide nanowires for electrochromic smart windows.

4

1.3 Organization of Thesis

This thesis will be written in a report that consists of several chapters. The chapters are as follow:

Chapter 1

Chapter 1 contains background and motivation of this research, as well as research gap and state of the art of the issues. This chapter also contains organization of research report.

Chapter 2

Chapter 2 explains basic theory whose relevancy with the research. This chapter also describes literature review and background of the research including tungsten oxide structure, electrochromic devices, electrochromic concept, and tungsten oxide based electrochromic device.

Chapter 3

Chapter 3 describes the experimental techniques employed in the present study to synthesis tungsten oxide for electrochromic devices.

5

Chapter 4

Chapter 4 discusses about the effect of heat-treatment temperature on structural, electrical, and electrochromic properties of tungsten oxide films for smart windows.

Chapter 5

Chapter 5 discusses about tungsten oxide nanowires for highly improved electrochromic smart windows.

Chapter 6

Chapter 6 contains conclusion of the research result and suggestion for the future research.

6

Chapter 2

Literature Review

This chapter explains basic theory whose relevancy with the research. This chapter also describes literature review and background of the research including tungsten oxide structure, electrochromic devices, electrochromic concept, and tungsten oxide based electrochromic device.

2.1 Introduction of Tungsten Oxide Materials

Tungsten is a transition metal, along with molybdenum, iridium, and nickel, found in Group VI of the Periodic Table of elements. At the same time, tungsten oxide, which is one of the transition metal oxides, has many interesting optical, electrical, structural, and chemical properties. Those interesting properties make it suitable for various technological applications such as catalysts [1], gas sensors [2], field emitters [3], or electrochromic devices [4-6].

Tungsten oxide structure has a nearly cubic structure which may be simply described as an "perovskite" type formed by WO_6 octahedron that share corners, with the O atoms at the corner and W atoms at the center of each octahedron, as shown in Fig. 2-1 [7-8]. This structure is also found for the material of rhenium trioxide (ReO_3)

7

and is commonly named as the ReO₃-structure (corner-sharing arrangement of octahedron). In fact, the symmetry of tungsten oxide is usually lower from the ideal ReO_3 structure due to the tilting of WO_6 octahedral structure or the displacement of tungsten from the center of its octahedral. Therefore, it results several transitions in the symmetry of structure, with the sequence of tetragonal → orthothombic → monoclinic → triclinic → monoclinic as the temperature is lowered from 900 to -189 ^0C [7]. Souza-Filho et al. have reported that the coexistence of triclinic and monoclinic phases of WO_3 is common at room temperature [9]. Moreover, it should be noted that the tungsten trioxide structure is likely host several kinds of defect. One of the most exist defect is the lattice oxygen vacancy, where the oxygen atom is absent from a normal lattice site. It causes the formation of WO_{3-x} compunds and influences the electric properties of non-stoichiometric tungsten oxides. Consequently, these oxygen vacancies lead donor-like effects for electrons and result in the n-type semiconducting properties of non-stoichiometric tungsten oxide [10].

8
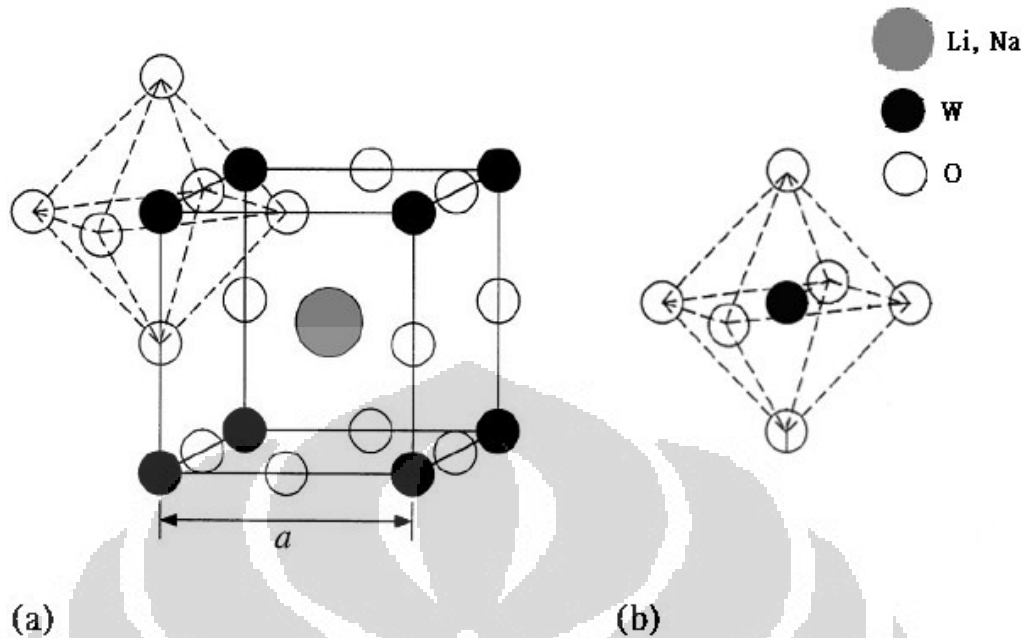
Figure 2-1. (a) Unit cell for the perovskite structure of (Li, Na) WO_3 (b) Octahedron

WO_6 symmetry [7-8].

2.2 Electrochromic Concept

2.2.1 Chromism, Electrochromism and Electrochromic Materials

Chromism, as a suffix, means "reversible change of color" [11]. It results from

a process caused by some form of stimulus. In most cases, chromism is based on

a change in the electron states of molecules, especially the π- or d-electron state,

so this phenomenon can be induced by various external stimuli which can alter

the electron density of substances [12].

9

Electrochromism is the reversible and visible change in transmittance and/or reflectance that is associated with an electrochemically induced oxidation–reduction reaction. It results from the generation of electronic absorption bands in the visible region, by switching between redox states [13].

An electrochromic material is a material that changes color in a persistent but reversible manner by an electrochemical reaction. These materials can exhibit different oxidation states, the color resulting from the electron delocalization between these states [14]. It is important to notice that for any electrochromic material to be able to exhibit electrochromism, it should be integrated in a system where potential application is possible [7].

Electrochromic materials can be divided into two main categories depending on the electron transfer process which results in the coloration, namely they are anodic and cathodic materials. Cathodic materials colour when they are reduced at a negative electrode while anodic materials are colored at an anode. Ti, Nb, Mo, Ta and W (typically group VI-B) oxides exhibit cathodic electrochromism while Ce, Mn, Fe, Co Ir, Rb and Ni (group VIII) oxides exhibit an anodic electrochromism [15].

A generalised form of the electrochromic reaction may be written as

$$\text{oxidized form, O} + \text{electron(s)} \rightarrow \text{reduced form, R}$$
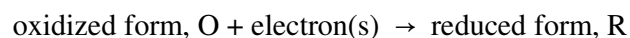
$$\text{color 1} \qquad\qquad\qquad \text{color 2}$$

where an electrode (O or R) acts as the source or sink of electron(s), e^- [13-15]. During the electrochromic reaction of metal oxides, the electrons responsible for the color enter or leave the metal oxide via the interface with the electrode while the ions necessary for charge balance ('electro-neutrality') enter or leave the film via the electrolyte [13]:

$$MO_y + x(H^+ + e^-) \rightarrow H_xMO_y$$
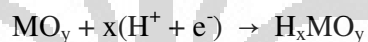
$$\text{color 1} \qquad\qquad \text{color 2}$$

where the mobile ion here is a proton, but Li^+ is another popular choice. The major color-forming phenomenon is an intervalence transition.

2.2.2   Electrochromic Properties

Diffusion coefficient, representing movement of mobile ions through electrochromic materials, is obtained from analysis of cyclic-voltammetric peak heights as a function of scan rate via the Randles–Servcik equation [16]:

11

$$D^{1/2} = \frac{i_p}{2.72 \times 10^5 \times n^{3/2} \times A \times C_o \times v^{1/2}}$$

where D is the diffusion coefficient (cm^2/s), i_p is the cathodic peak current density (A/cm^2), n is the number of electrons, A is area of the film (cm^2), C_o is the electrolyte concentration (mol/cm^3), and v is the scan rate (V/s).

The Coloration Efficiency is an important property to compare the efficiency of electrochromic layers. It is also called electrochromic efficiency and has the units cm^2/C. It is defined as

$$CE = \frac{\Delta OD(\lambda)}{\Delta Q}$$

where ΔOD (λ) represents the change in optical density at the wavelength λ, resulting from ΔQ charge transferred to the electrochromic materials.

The Optical density (OD) is an expression of the optical transmittance of an element at a given wavelength and is expressed as ln (T_b/T_c) where T_b and T_c are the transmittance of electrochromic materials in its respective bleached and colored state at the wavelength λ.

Response time is the time required for an electrochromic device to change from its bleached to its coloured state (or vice versa). It is generally unlikely that response times for coloration (t_c) equal to response times for bleaching (t_b).

12

2.2.3   Electrochromic Devices

Electrochromic device contain four primary layers: (1) electrochromic (active) layer; (2) ion conductor (electrolyte) layer; (3) ion storage layer; and (4) transparent conductor layer [7]. Figure 2-2 shows structure of an electrochromic device.

A voltage applied between the transparent electrodes leads to charge being shuttled between the electrochromic and ion storage layers, and the overall transparency is thereby changed. A voltage with opposite polarity—or, with suitable material combinations, short circuiting—makes the device regain its original properties. The optical modulation requires a DC voltage of as little as 1–3 V. The charge insertion into the electrochromic layer is balanced by electron inflow from the transparent conductor layer; these electrons can make intervalency transitions (i.e., yield polaron absorption), which then is the basic reason for the optical absorption [17].

13
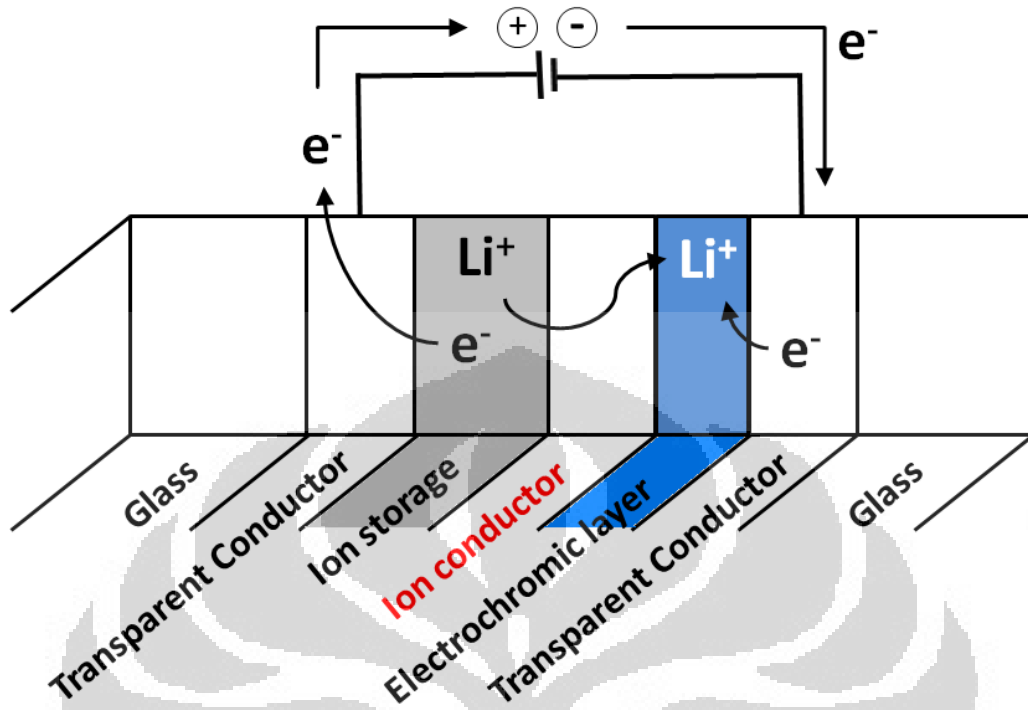
Figure 2-2. Structure of an electrochromic device. Arrows indicate the transport of Li^+ ions compensated by electron flow from adjacent transparent conductor layer; figure adopted from [17].

In fact, there are four different fields within which electrochromic devices offer distinct advantages over alternative technologies; they are schematically represented in Figure 2-3 [18]. The smart window in Fig. 2-3(a) is able to change their optical property in response to an external voltage. Such windows are likely to have important applications in innovative and energy-efficient architecture

14

where they would adjust the inflow of luminous radiation and solar energy through glazings in buildings and large atria. Smart windows may eventually have a profound influence on architecture and lead to new design philosophies with window apertures and wall claddings having regulatory functions, thus making buildings perform intelligently in concert with their ambience.

By replacing one of the transparent electrical conductors of the smart window with a specularly reflecting metallic reflector, one reaches the variable-reflectance device of Fig. 2-3(b). Its applications include anti-dazzling rear view mirrors for cars and trucks. If one integrates a white pigment in the electrochromic device, it can serve for information display purposes as depicted in Fig. 2-3(c). The black/white contrast and off-normal viewing properties can be excellent, holding promise for important applications in "signs" and "labels" of different kinds. Another possible device area concerns surfaces with variable thermal emittance, as sketched in Fig. 2-3(d); such surfaces are of interest for temperature stabilization of satellites.

15
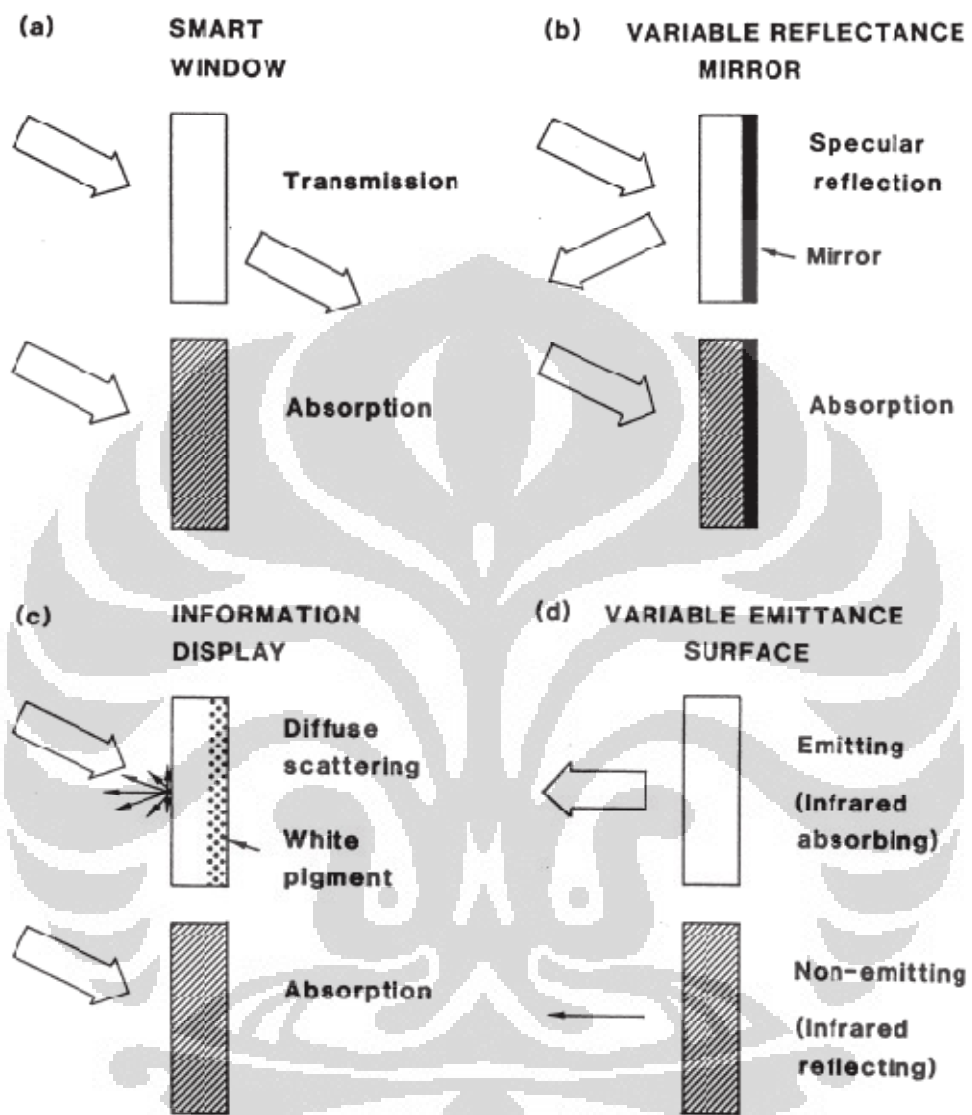
Figure 2-3. The principles of four different applications of electrochromic

devices. Arrows indicate incoming and outgoing electromagnetic radiation

intensity [18].

16

2.3 Tungsten Oxide Based Electrochromic Devices

Recently, many transition metals oxide, e.g. cobalt, iridium, molybdenum, nickel, rhodium, tungsten, vanadium, etc., have been shown to possess electrochromic property [15]. The transition metal oxide can change their colors due to optical intervalence charge transfer. The intervalence colored forms of most transition-metal oxide electrochromes are in the range blue or grey through to black; it is much less common for transition-metal oxides to form other colours by intervalence transitions (see Table 2.1) [15].

However, among the numerous transition metal oxides, tungsten oxide, are of intense interest due to the most intense electrochromic color changes have been investigated extensively in several books [7,15] and review articles [8,19]. Other metal oxides of lesser colorability are therefore more useful as optically passive, or nearly passive, counter electrodes [15].

17

Table 2.1. Summary of the colours of metal-oxide electrochromes.[15]

Metal	Oxidised form[a] *of oxide*	Reduced form[a] *of oxide*
Cobalt	$LiCoO_2$ Pale yellow-brown	M_xLiCoO_2 (M≠Li) Dark brown
Iridium	$Ir(OH)_3$ Colorless	$IrO_2.H_2O$ Blue-grey
Molybdenum	MoO_3 Colorless	M_xMoO_3 Intense blue
Nickel	$Ni^{II}O_{(1-y)}H_z$ Brown-Black	$Ni^{II}_{(1-x)}Ni^{III}_xO_{(1-y)}H_{(z-x)}$ Colorless
Rhodium	Rh_2O_3 Yellow	RhO_2 Dark green
Tungsten	WO_3 Very pale yellow	M_xWO_3 Intense blue
Vanadium	V_2O_5 Brown-yellow	$M_xV_2O_5$ Very pale blue

[a]The counter cation M is lithium unless stated otherwise.

18

Chapter 3

Experimental Procedure

This chapter describes the experimental techniques employed in the present study to synthesis tungsten oxide for electrochromic smart windows. In this study, tungsten films were deposited on ITO Glass substrates by RF magnetron sputtering system. The as-prepared tungsten films were subsequently treated by Thermal-Chemical Vapor Deposition (T-CVD). Furthermore, the microstructure, electrical, optical, and electrochromic properties of grown tungsten oxides were characterized by various analytical instruments. Figure 3-1 shows the experimental procedure and analytical instruments used in this study.
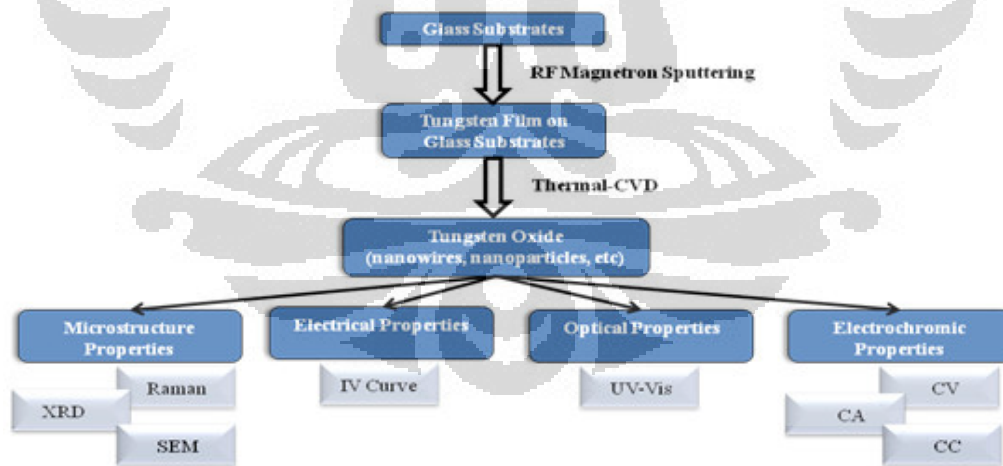
Figure 3-1. Experimental Procedure and Analytical Instruments

3.1 Synthesis of Tungsten Oxide Film

In this study, thin films of tungsten were deposited on cleaned indium tin oxide (ITO) glass substrates by RF magnetron sputtering system. The as-prepared tungsten films were subsequently oxidized for different heat-treatment by Thermal-Chemical Vapor Deposition (T-CVD). This has attracted much attention due to the simplicity of the technique and high crystallinity of the products [1].

3.1.1 Cleaning of the Substrates

The glass substrates (glass coated with ITO, 5 $\Omega/\square$) with 0.7 mm thick were cut into small pieces with the specific size of 2 cm (width) x 2 cm (length). These substrates were ultrasonically cleaned using ethanol (C_2H_5OH) and deionized water (Delta Ultrasonic Cleaner; 20 min). The ultrasonic cleaning was followed by nitrogen jet spray to achieve removal of particles from the substrates. The glass substrates cleaning procedure is shown in Fig. 3-2.

Figure 3-2. The glass substrates cleaning procedure

20

3.1.2 Tungsten Thin Film Deposition

Tungsten thin films were deposited on ITO glass substrates by RF magnetron sputtering system, manufactured by the Gordon Technology. A tungsten target used in this experiment has a diameter of 2 inches of pure tungsten target (99.5%). In addition, the chamber vacuum system consists of 2 pumps, mechanical pumps and high vacuum diffusion pump. The mechanical pumps used for pumping the sputtering chamber until the pressure about 4×10^{-2} Torr and followed by the high vacuum diffusion pump to vacuum the chamber in high vacuum pressure about 2×10^{-5} Torr. The samples were then generated at an argon flow rate of 25 sccm and working pressure of 2.1×10^{-2} Torr. The deposition process was conducted for various sputtering time and RF power. Prior to the deposition process, pre-sputtering was performed for about 5 min to clean the target surface. The magnetron sputtering system is shown in Fig. 3-3.

21
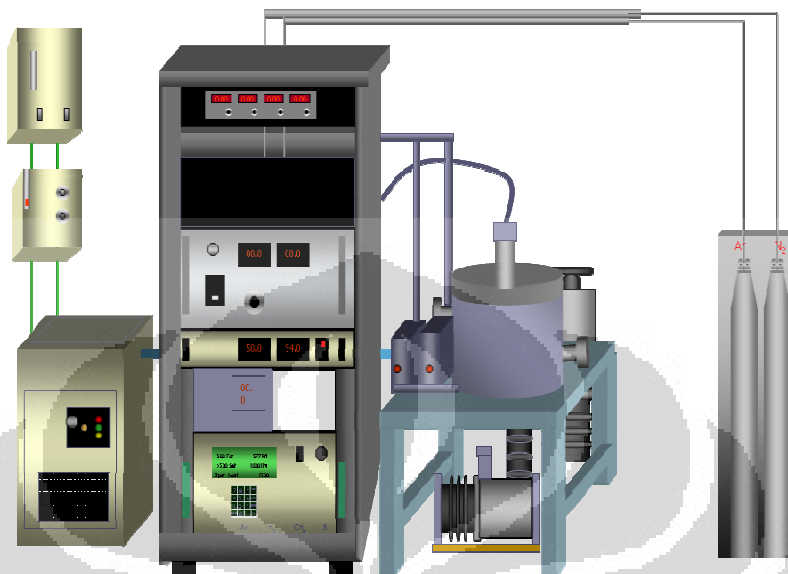
Figure 3-3. The magnetron sputtering system

3.1.3   Tungsten Oxide Film by Heat-Treatment Technique

The as-deposited tungsten films were subsequently thermally oxidized at three different heat-treatment temperatures (450 ^{o}C, 550 ^{o}C, and 650 ^{o}C) in Ar and O_2 ambient. The deposited samples were first loaded into a vacuum condition and placed in the middle of a quartz tube furnace. The samples were then heated to the desired temperatures in the total pressure of ~50 Torr for 2 hours with a continuous flow Ar/O_2 feed gas composition ratio of 10:1, as shown in Fig. 3-4. The samples were then cooled in the furnace to room temperature over ~4 hours.

22
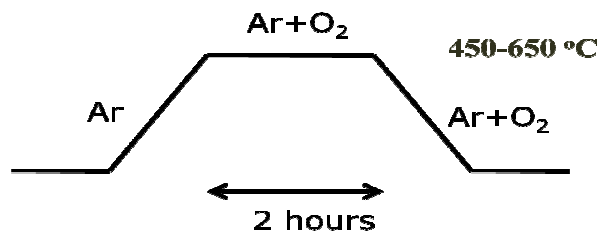
Figure 3-4. Heat treatment experimental details

3.1.4 Tungsten Oxide Nanowires by Two-Step Heat-Treatment Technique

The reaction for growth of tungsten oxide nanowires was carried out in a horizontal quartz tube furnace at various heat-treatment temperatures ranging from 400 ^{o}C , 500 ^{o}C , 600 ^{o}C, and 700 ^{o}C. For the first step, the as-deposited tungsten film samples were loaded into a vacuum condition and placed in the middle of a quartz tube furnace. The samples were then heated from 400 to 700 ^{o}C in the total pressure of approximately 50 Torr for 1 hour with a continuous nitrogen flow of 150 sccm. Then, the samples were cooled in the furnace to room temperature. The final step, the annealed samples were oxidized with a continuous O_2 flow of 10 sccm at 450 ^{o}C for 30 min to grow tungsten oxide nanowires, as shown in Fig. 3-5. The samples were then cooled in the furnace to room temperature over ~4 hours.

23

N_2 400-700 °C

N_2 N_2/150 sccm N_2

O_2 450 °C

O_2 O_2/10 sccm O_2

1 hour

30 min
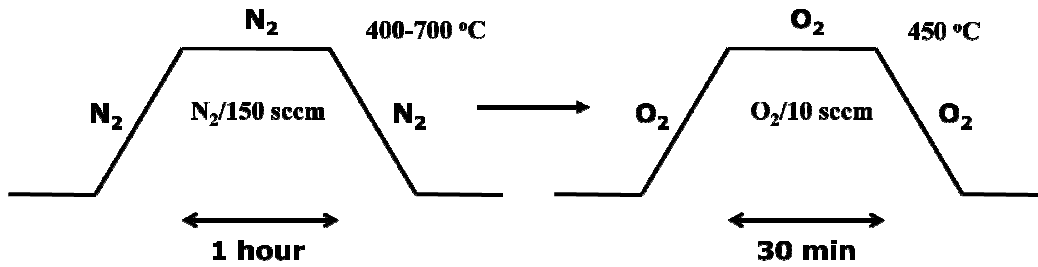
Figure 3-5. Two-step heat treatment experimental details

3.2 Characterization

The surface morphology and microstructure properties of tungsten oxide films were characterized by Raman Spectroscopy, X-ray diffraction (XRD), and Field Emission Scanning Electron Microscopy (FESEM). The electrical and optical properties were characterized by (Current-Voltage) I-V and optical transmittance spectra measurement system, respectively. The electrochromic properties were characterized by Cyclic Voltametry (CV).

3.2.1 Raman spectroscopy

Raman spectroscopy is a vibrational technique using an indirect coupling of high-frequency radiation, such as visible light, with vibrations of chemical bonds. Raman spectrum is very sensitive to the lengths, strengths and arrangements of chemical bonds in a material, but less sensitive to the chemical composition. When the incident photon interacts with the chemical bond, the chemical bond is

24

excited to a higher energy state. Most of the energy would be re-radiated at the same frequency as that of the incident exciting light, which is known as the Rayleigh scattering [2]. In this study, the Raman spectrum were obtained by a Raman Spectroscopy with the wavelength of 532 nm, laser power of 5 mW and beam size of 5 μm.

3.2.2   X-ray diffraction (XRD)

XRD is a very important experimental technique that has been widely used for the determination of crystallinity, crystal structures and lattice constants of nanoparticles, nanowires and thin films [2]. XRD is nondestructive and does not require elaborate sample preparation. A collimated beam of X-rays, with a wavelength typically ranging from 0.7 to 2 Å, is incident on a specimen and is diffracted by the crystalline phases in the specimen according to Bragg's law [3]:

$$\lambda = 2d \sin\theta$$

where d is the spacing between atomic planes in the crystalline phase and λ is the X-ray wavelength. The intensity of the diffracted X-rays is measured as a function of the diffraction angle 2θ and the specimen's orientation. This diffraction pattern is used to identify the specimen's crystalline phases and to

25

measure its structural properties. In this study, the XRD pattern was recorded on a 2θ configuration using Bruker D8 Discovery X-ray diffractrometer with non-monochromated Cu Kα X-ray radiation (λ= 1.54056 Å).

3.2.3   Field Emission Scanning Electron Microscopy (FESEM)

The scanning electron microscope (SEM) permits the observation and characterization of heterogeneous organic and inorganic materials on a micrometer (μm) to nanometer (nm) scale. A major reason for using SEM is the high resolution and not destructive.

Electron gun in SEM provides a stable beam of electrons of adjustable energy. The electron sources described so far rely on the use of high temperatures to enable electrons in the cathode to overcome the work function energy barrier and escape into the vacuum. These thermionic sources are relatively inexpensive and need no special vacuum, but have the disadvantages of low brightness, limited lifetime, and large energy spread. Field emission is an alternative way of generating electrons which is free of these [4]. In this study, the surface morphology of the tungsten oxide films was visualized by JEOL JSM-6500F Field Emission Scanning Electron Microscopy (FESEM).

26

3.2.4   Current-Voltage (I-V) Measurement System

In this study, a Keithley 237 current-voltage (I-V) measurement system was used for the resistance measurement. An external computer such as the PC computer controller is required to control this measurement. Ohm's law is used in order to determine a resistance: R=V/I. A known current is sourced and flows through the unknown resistance. We measure the voltage that develops across the resistance by dividing the measured voltage by the sourced current.

3.2.5   Optical Transmittance Spectra Measurement System

Optical spectrophotometer can precisely measure transmittance and reflectance spectra over a wide range of wavelengths. The optical transmittances spectra were recorded on a JASCO V-560 UV-Vis spectrophotometer in the wavelength range of 300-800 nm. The JASCO V-560 UV-Vis spectrophotometer allows nondestructively measuring and performs spectrophotometric measurements across a wide wavelength range from the ultraviolet to the infrared.

In this study, the optical transmission spectra recorded for all samples in their bleached and colored states. The transmittance difference (ΔT) and the

27

change in optical density (ΔOD) between the bleached and colored states at certain wavelength are respectively calculated using relations.

$$\Delta T = \left[\frac{T_b}{T_c}\right]$$

$$\Delta OD = ln\left(\frac{T_b}{T_c}\right)$$

where T_b and T_c are the transmittance of the electrochromic materials in its respective bleached and colored states at certain wavelength.

3.2.6   Cyclic Voltametry (CV)

Cyclic voltammetry (CV) is a type of potentiodynamic electrochemical measurement that working electrode potential is ramped linearly versus time like linear sweep voltammetry. In this study, the CV cell contains the solutions of 1M lithium perchlorate (LiClO$_4$) in propylene carbonate (PC)-water mixtures as the electrolytes, a platinum plate as the counter electrode (CE), tungsten oxide as the working electrode (WE), and saturated calomel electrode (SCE) as the reference electrode (RE). Figure 3-6 shows schematic representation of three electrode cell used in electrochemical characterization.

To characterize the working electrode (WE), a current is passed through the electrode in a controllable way by applying a potential to the electrode that is

28

different from the equilibrium potential. The potential of the working electrode (WE) is measured against the reference electrode (RE). The current is allowed to pass through counter electrode (CE) to complete the current flow circuit. The potential difference between working electrode and reference electrode is controlled by means of a potentiostat.

To characterize the working electrode (WE), a current is passed through the electrode in a controllable way by applying a potential to the electrode that is different from the equilibrium potential. The potential of the working electrode (WE) is measured against the reference electrode (RE). The current is allowed to pass through counter electrode (CE) to complete the current flow circuit. The potential difference between working electrode and reference electrode is controlled by means of a potentiostat.

29
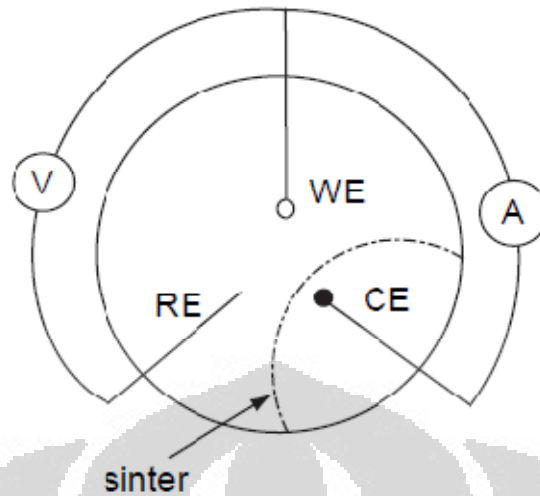
Figure 3-6. Schematic representation of three electrode cell used in electrochemical characterization. A platinum plate as the counter electrode (CE), tungsten oxide as the working electrode (WE), and SCE as the reference electrode (RE). [5].

Figure 3-7 shows a schematic cyclic voltammogram (CV). The CV experiment involves applying a potential smoothly varying with time t, over a range including the electrode potential $E_{O,R}$ of the WE and observing the resultant current, which will peak (with value I_p) near $E_{O,R}$. A widely used application involves the Randles–Sevcik equation linking the peak current I_p with concentration C_o, v and the diffusion coefficient D. D is dealt with in further detail in Chapter 2:

$$D^{1/2} = \frac{i_p}{2.72 \times 10^5 \times n^{3/2} \times A \times C_o \times v^{1/2}}$$

30

The other symbols have already been defined.
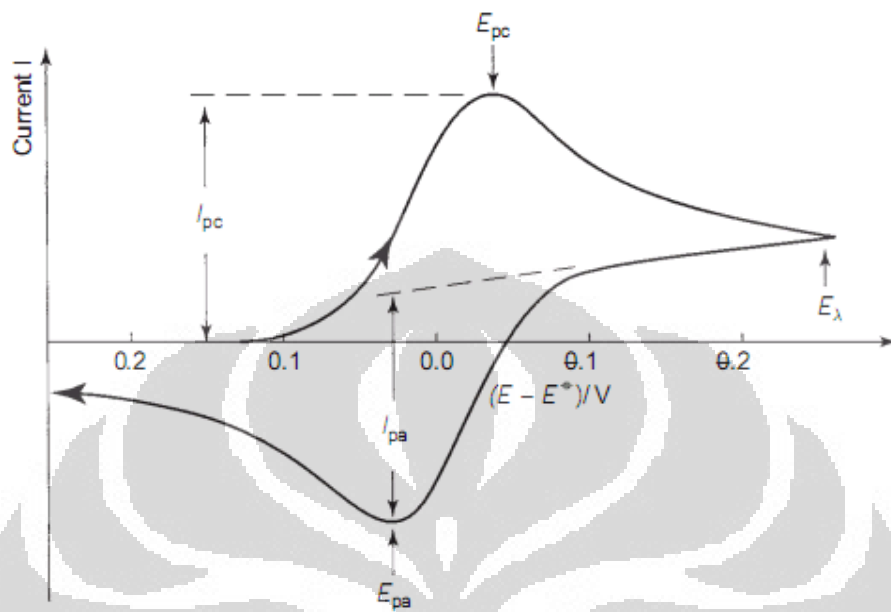
Figure 3-7. Schematic cyclic voltammogram for a simple, reversible, one-electron redox couple, in which all species remain in solution [5].

3.2.7   Chronoamperometry (CA)

Chronoamperometry (CA) is an electrochemical technique in which the potential of the working electrode is stepped and the resulting current (ampere) from faradic processes occurring at the electrode (caused by the potential step) is monitored as a function of time (crono).

31

The response to a potential step is current due to the electrolysis of Oxidation or Reduction. Hence, it is instructive to first consider the current vs. time experiment, as shown in Fig. 3-8. The analysis of chronoamperometry (CA) data is based on the Cottrell equation, which defines the current-time dependence for linear diffusion control:

$$i = \frac{nFACD^{1/2}}{\pi^{1/2}t^{1/2}}$$

where n is the number of electrons transferred, F is the Faraday's constant (96,485 C/mol), A is the electrode area (cm^2), D is the diffusion coefficient (cm^2/s), and C is the the electrolyte concentration (mol/cm^3). This indicates that, under these conditions, there is a linear relationship between the current and the 1/square root of time. A plot of i vs. $t^{-1/2}$ is often referred to as the Cottrell plot.

3.2.8 Chronocoulometry (CC)

Chronocoulometry (CC) is an electrochemical technique in which the potential of the working electrode is stepped and the resulting charge (coulombs) from faradic processes occurring at the electrode (caused by the potential step) is monitored as a function of time.

32

The response to a potential step is charge due to the electrolysis of Oxidation or Reduction. Hence, it is instructive to first consider the charge vs. time experiment, as shown in Fig. 3-8. The analysis of chronocoulometry (CC) data is based on the Anson equation, which defines the charge-time dependence for linear diffusion control:

$$Q = \frac{2nFACD^{1/2}}{\pi^{1/2}} t^{1/2}$$

where n is the number of electrons transferred, F is the Faraday's constant (96,485 C/mol), A is the electrode area (cm^2), D is the diffusion coefficient (cm^2/s), and C is the the electrolyte concentration (mol/cm^3).

33
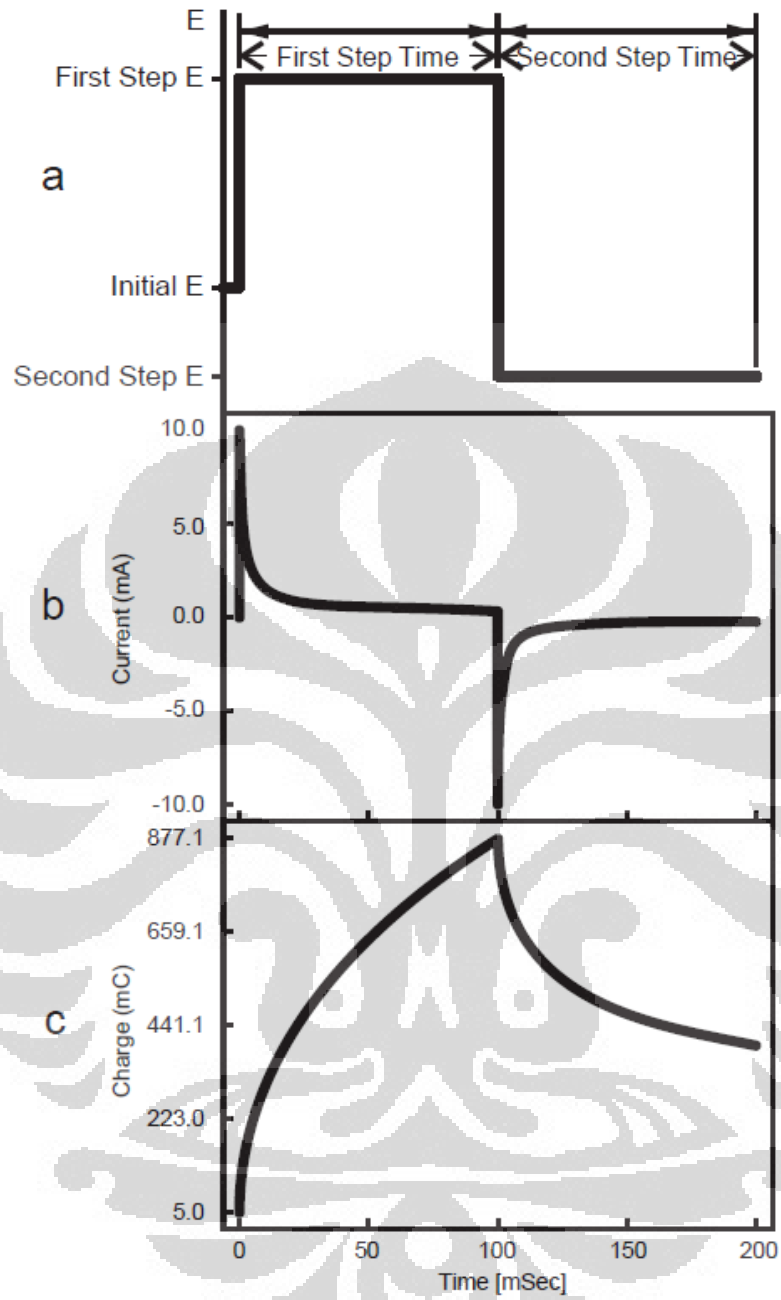
Figure 3-8. Potential wave form of (a) the double potential step technique,

(b) the current response, and (c) the charge response [6].

34

Chapter 4

Effect of Heat-Treatment on the Properties of Tungsten Oxide Thermally Oxidized Films for Electrochromic Smart Windows

4.1. Experimental details

Tungsten films were deposited onto indium tin oxide (ITO) glass substrates by RF magnetron sputtering system. ITO glass substrates were cut into small pieces with the specific size of 1.5 cm (width) x 1.5 cm (length). These substrates were ultrasonically cleaned using ethanol and deionized water (Delta Ultrasonic Cleaner; 20 min). The ultrasonic cleaning was followed by nitrogen jet spray to achieve removal of particles from the substrates.

The sputtering system used pure (99.99%) tungsten as a target and pure (99.99%) argon as the sputtering gas with a base chamber pressure of ~3×10^{-5} Torr. Prior to the deposition process, pre-sputtering was performed for about 5 min to clean the target surface. The samples were then generated at an argon flow rate of 25 sccm (standard cubic centimeter per minute) and an RF power of 150 W for 3 min. The thickness of the tungsten films were ~100 nm.

The as-deposited tungsten films were subsequently thermally oxidized at three different heat-treatment temperatures (450 ^{o}C, 550 ^{o}C, and 650 ^{o}C) in Ar and O_2 ambient. The deposited samples were first loaded into a vacuum condition and placed in the middle of a quartz tube furnace. The samples were then heated to the desired temperatures in the total pressure of ~50 Torr for 2 hours with a continuous flow Ar/O_2 feed gas composition ratio of 10:1. The samples were then cooled in the furnace to room temperature over ~4 hours.

The surface morphology of the thermally oxidized films was visualized by a JEOL JSM-6500F field emission scanning electron microscope (FESEM) at 15 kV. The crystallinity of the

samples was characterized by X-ray diffraction (XRD) recorded at a 2θ configuration using a Bruker D8 Discovery X-ray diffractrometer with non-monochromated Cu Kα X-ray radiation (λ= 1.54056 Å). The 2θ investigation region was in the 20°-70° range with a scanning speed of 2 degrees/s. In addition, the electrochemical intercalation and deintercalation of the samples was carried out in a potentiostat controlled by a personal computer in a three electrode cell configuration with 1 M lithium perchlorate ($LiClO_4$) in a propylene carbonate (PC)-water mixture as the electrolytes, a platinum plate as the counter electrode, tungsten oxide as the working electrode and the saturated calomel electrode (SCE) as the reference electrode. A Keithley 237 electrometer was used for the electrical resistance measurement. Optical transmittances spectra were recorded on a JASCO V-560 UV-Vis spectrophotometer in a wavelength range of 390-800 nm. The transmission spectra switch of a thermally oxidized tungsten film was examined in the spectral region between 390 and 800 nm by applied coloring/bleaching voltage (- 3.5 V/ +2.0 V).

4.2. Effect of heat-treatment on structural properties

Figure 4-1 shows the XRD pattern of the crystal phase transformation of the as-deposited and thermally oxidized tungsten films at three different heat-treatment temperatures. The XRD pattern of the as-deposited tungsten film on ITO glass substrate (Fig. 4-1a) displays three diffraction peaks at 2θ = 37.5^{o}, 39.8^{o}, and 45.5^{o}, which could be well indexed to a β-W phase (cell constants: a = 5.05 Å; JCPDS Card 47-1319). These three peaks are assigned to the (200), (210), and (211) crystallographic planes of the β-W phase. Chen et al., showed that, based on the experimental conditions, the lattice parameter of β-W varies from 0.496 to 0.518 nm [1]. These reported values are in line with our obtained results. In addition, the diffraction peaks exhibit the broadened peaks of the 2θ region (33-46°) which indicates that the crystalline structure of the as-deposited tungsten film coexists with an amorphous phase.

Figure 4-1. XRD patterns of (a) as-deposited and thermally oxidized tungsten film at three different heat-treatment temperatures: (b) 450 ^{o}C, (c) 550 ^{o}C, and (d) 650 ^{o}C.

Further heat-treatment at 450 °C and 550 °C (Figs. 4-1b and c) resulted in the formation of tetragonal WO_3 (lattice constants: a = 5.250 Å, c = 3.919 Å; JCPDS Card 85-0807) as indicated by the presence of three diffraction peaks at $2\theta = 22.7°$, $23.9°$ and $33.1°$, corresponding to the (001), (110), and (111) lattice planes. These results are comparable with the XRD analyses on WO_3 films heated to 500°C after being cast by the chemical vapor deposition (CVD) method, which also showed a tetragonal WO_3 phase [2]. Both the thermal oxidization samples also show the (110) plane appears with relatively higher intensity. The only detectable difference between the two samples is the stronger intensity and narrowing of the diffraction peak at $2\theta = 23.9°$ when the heat-treatment temperature is 450 °C. This suggests that the 450 °C sample has better crystallinity than the 550 °C sample. Finally, a heat-treatment temperature at 650 °C (Fig. 4-1d) results in the disappearance of the tetragonal WO_3 phase peaks and the emergence of new peaks at $2\theta = 23.5°$, $23.8°$, and $24.4°$. These peaks are assigned to the (010), (103), and (502) lattice planes of the monoclinic $W_{18}O_{49}$ phase (lattice constants: a = 18.32 Å, b = 3.784 Å, c = 14.035 Å, β = 115.20°; JCPDS Card 36-0101). Multiple sharp peaks appeared in the thermal oxidization sample when the temperature is increased to 650 °C. This phenomenon was identified as a residual stress in the tungsten film at higher temperatures [3]. However, the 650 °C sample also results in the phase transition from tetragonal WO_3 to monoclinic $W_{18}O_{49}$. Moulzolf et al. [4] also obtained a monoclinic phase for WO_3 film RF sputtered at 650 °C in deposition.

Figure 4-2 shows the SEM images for the surface morphology of the as-deposited and the thermally oxidized tungsten films at three different heat-treatment temperatures. As seen in Fig. 4-2a, the as-deposited tungsten film has a smooth surface and no grains. However, when the thermal oxidization temperature was increased to 450 °C (Fig. 4-2b), nanoparticles with spherical grains diameters of ~40 nm are clearly seen. This SEM result is consistent with the narrowing of the diffraction peaks on XRD patterns as a result of increasing heat-treatment temperatures [5]. As shown in Figs. 4-2c and d, nanoparticles with spherical grains diameters of ~55 nm and 80-100 nm were

grown on the thermally oxidized tungsten film at 550 $^{\circ}$C and 650 $^{\circ}$C, respectively. In addition, the heat-treatment temperature at 550 $^{\circ}$C had a uniform and dense surface morphology of tungsten oxide film. When the temperature is increased to 650 $^{\circ}$C, the grain size is the largest. The grain size increases due to the growth and agglomeration of grains at higher heat-treatment temperature [6]. Furthermore, the surface roughness of the 650 $^{\circ}$C is higher than those of the 450 $^{\circ}$C and 550 $^{\circ}$C samples, as shown in Figs. 4-2. Consequently, increasing the oxidization temperature not only increases the grain size but also increases the surface roughness of the tungsten oxide films. The effects of the thermal oxidization of as-deposited tungsten film on the tungsten oxide surface morphology and crystal phase are described in Table 4-1.
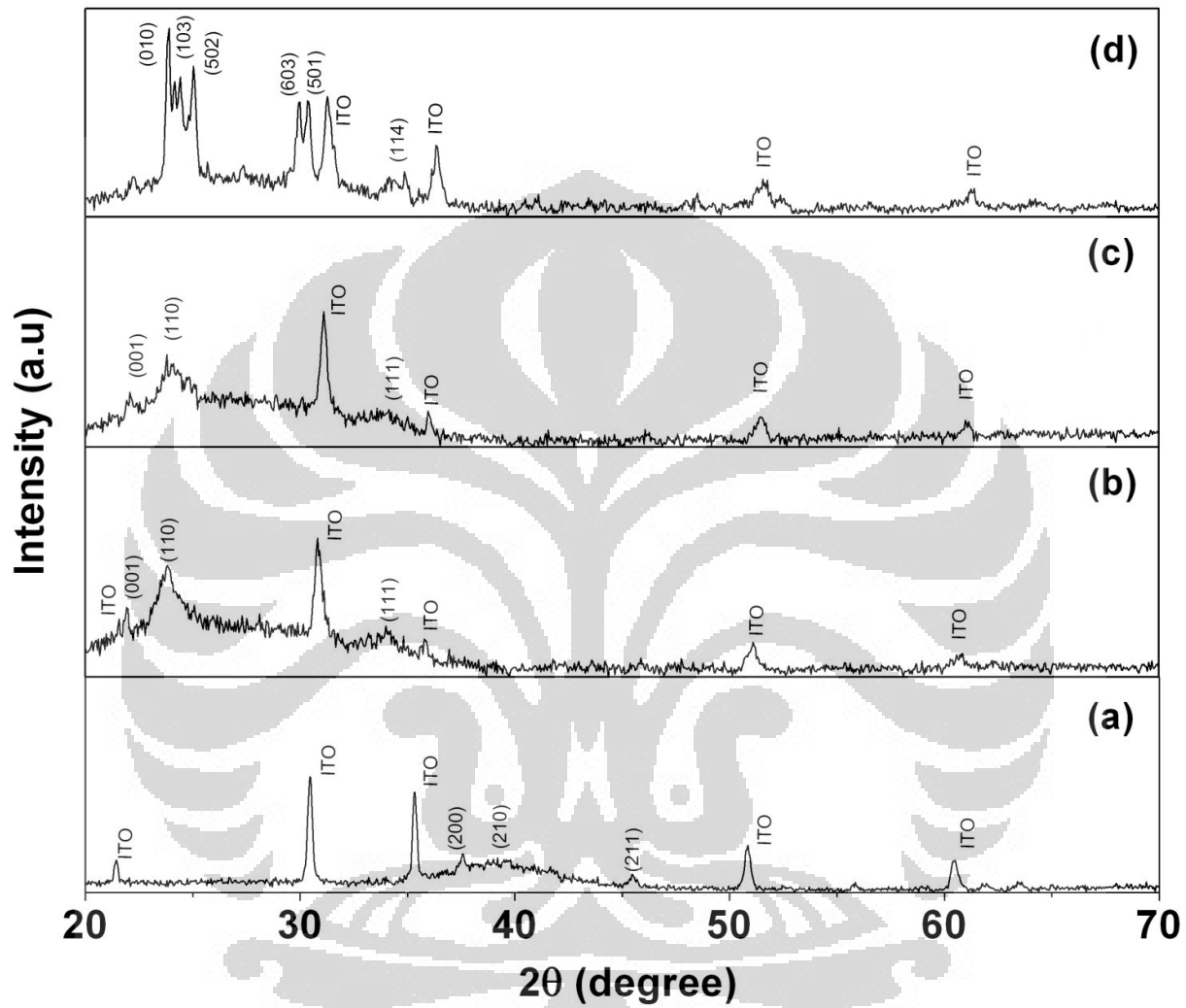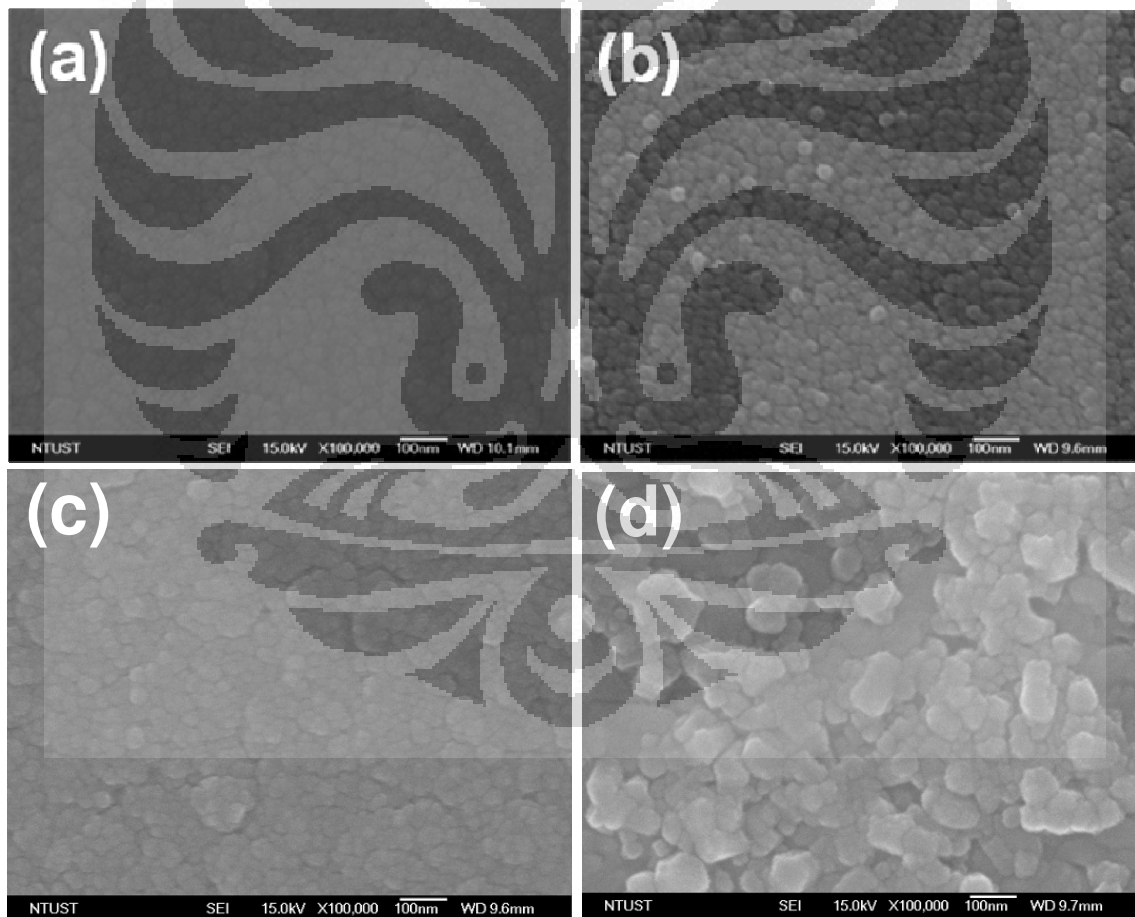

Figure 4-2. SEM images of (a) as-deposited and thermally oxidized tungsten films at three different heat-treatment temperatures: (b) 450 $^{\circ}$C, (c) 550 $^{\circ}$C, and (d) 650 $^{\circ}$C.

39

Table 4-1. Effect of heat-treatment on tungsten oxide surface morphology and crystal phase

Thermal condition	Surface morphology	Crystal phase (Crystal structure; lattice constants; space groups)
As-deposited	Smooth crystalline surface and no grains	Cubic β-W; a = 5.05 nm; Pm3n
450 ^{o}C	Nanoparticles with spherical grains (~40 nm)	Tetragonal WO_3; a = 5.250 Å, c = 3.919 Å; P4/nmm
550 ^{o}C	Nanoparticles with spherical grains (~55 nm)	Tetragonal WO_3; a = 5.250 Å, c = 3.919 Å; P4/nmm
650 ^{o}C	Nanoparticles with spherical grains (80-100 nm)	Monoclinic $W_{18}O_{49}$; a = 18.32 Å, b = 3.784 Å, c = 14.035 Å, β = 115.20^{o}; P2/m

4.3 Effect of heat-treatment on electrical property

Figure 4-3 show electrical measurement of the thermally oxidized tungsten films at three different heat-treatment temperatures. Tungsten oxide thin films show the variation from highly conductive to a high-resistive one at three different heat-treatment temperatures. As seen in Fig. 3, the conductivity of thermally oxidized tungsten film increase continuously up to 550 ^{o}C and then decrease till 650 ^{o}C. According to Alam et al. [7] with increasing annealing temperature, the ITO thin films would perform higher resistivity. As observe in the SEM, the films exhibit the grain-like structure. The grain size increases due to the growth and agglomeration of grains at higher heat-treatment temperature [6]. Thus, the increase in conductivity of heat-treatment temperature at 550 ^{o}C may be due to various processes such as agglomeration of grains, uniform and dense surface morphology, etc. leading to evolution of tungsten–oxygen networks.
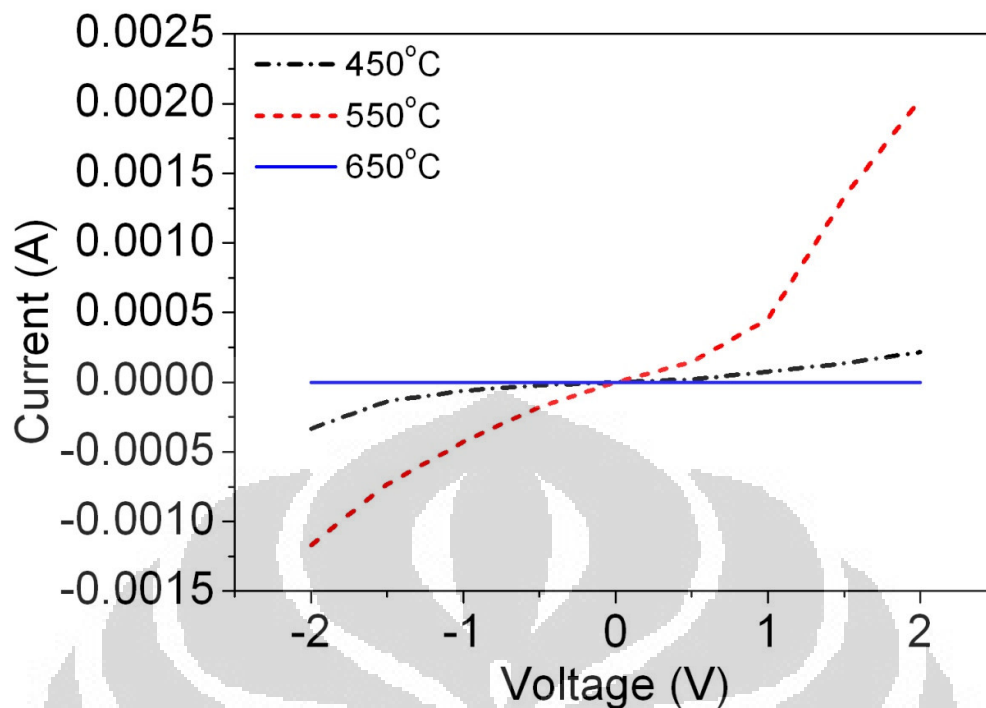
Figure 4-3. I-V measurements of thermally oxidized tungsten films at three different heat-treatment temperatures: 450 °C, 550 °C, and 650 °C.

4.4 Effect of heat-treatment on electrochromic properties

Figure 4-4 shows cyclic voltammograms recorded at a 100 mV/s scanning rate with a linear potential sweep of -1 to 1 V (Versus SCE) for thermally oxidized tungsten film at three different heat-treatment temperatures. The cathodic peak current (I_{pc}) and anodic peak current (I_{pa}) values are given in Table 4-2. The current recorded is due to a cation intercalation/deintercalation according to the reaction

$$WO_3(bleach) + xLi^+ + xe^- \leftrightarrow Li_xWO_3(blue) \tag{1}$$

where Li$^+$ is ion in the lithium perchlorate organic solution. The integrated cathodic-current density equates to the amount of lithium ions intercalated to form a tungsten bronze.

41

Figure 4-4 shows that the voltammogram area, hence the charge storage capacity, is maximized in the 550 °C sample, followed by 450 °C and 650 °C samples. The absolute value of peak current density is an indication of the electrochemical activity of the working electrode [8]. The results presented in Table 4-2 show that the value of the peak current (I_{pc} and I_{pa}) is highest in the 550 °C sample. Furthermore, the insertion efficiencies for these samples are determined by diffusion coefficients calculated using the well-known Randles-Servcik equation [9]

$$D^{1/2} = \frac{i_p}{2.72 \times 10^5 \times n^{3/2} \times A \times C_o \times v^{1/2}} \tag{2}$$

where i_p is the cathodic peak current, $n=1$ is the number of electrons, A is area of the film, C_o is the electrolyte concentration (1 M), and v is the scan rate. Calculated values are given in Table 4-2. The diffusion coefficient of 1.7×10^{-11} cm^2/s for the 550 °C sample is the largest, closely followed by the diffusion coefficient of 5.2×10^{-12} cm^2/s for the 450 °C sample. The lowest diffusion coefficient of 4.1×10^{-14} cm^2/s is found in the 650 °C sample, which is a natural consequence of its peak current. Therefore, the sample oxidized at 550 °C has the greatest electrochemical activity and diffusion coefficient, may be due to the highest conductivity of tungsten oxide film thermally oxidized at 550 °C which allows for the easy transport of ions across the film and thus enhances the peak current.
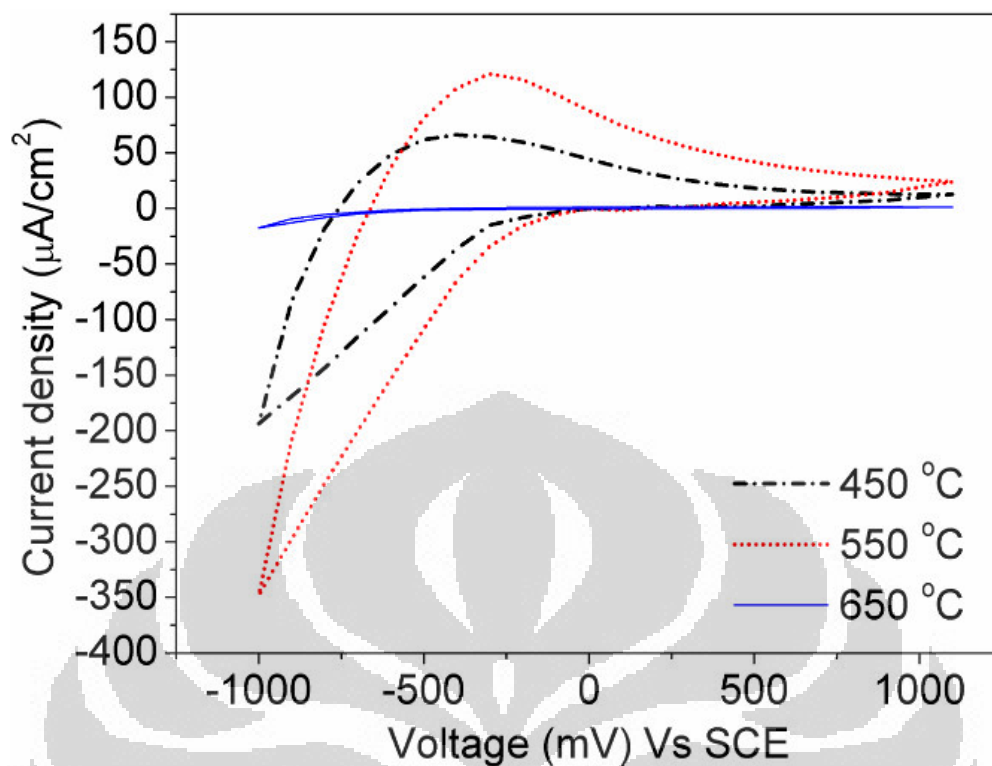
Figure 4-4. Cyclic voltammograms spectra for thermally oxidized tungsten films at three different heat-treatment temperatures: 450 ^{o}C, 550 ^{o}C, and 650 ^{o}C.

Table 4-2. Effect of thermal oxidization on electrochromic performance

Heat-treatment condition	I_{pc} ($\mu A/cm^2$)	I_{pa} ($\mu A/cm^2$)	Diffusion coefficient (cm^2/s)	Reversibility (%)
450 ^{o}C	194	66.4	5.2×10^{-12}	10.4
550 ^{o}C	348	121	1.7×10^{-11}	45.1
650 ^{o}C	17.4	1.3	4.2×10^{-14}	1.4

Figure 4-5 shows typical chronoamperometric (CA) traces recorded during coloration and bleaching of the thermally oxidized tungsten film at three different temperatures. During the experiment, CA cycling was performed on the thermally oxidized tungsten film between +1 and -1 V (versus SCE). The voltage was stepped from 0 to -1 V for 10 s (coloration) and then reversed to

43

+1 V for the next 10 s (bleaching). The CA technique was used to measure the response time for the thermally oxidized tungsten film. Response times for coloration (t_c) and bleaching (t_b) were calculated from current time transients. The plots suggest that the response time is the fastest for 450 ^{o}C sample (coloration time 1.6 s, bleaching time 1.2 s) and closely followed by 550 ^{o}C (coloration time 2 s, bleaching time 1.5 s). However, response time for thermally oxidized tungsten film at 650 ^{o}C could not be calculated because of the small current peak density value. The best response time exhibit in the tetragonal WO_3 films (450 ^{o}C and 550 ^{o}C samples), possibly because the sample's higher conductivity allows for easy transport of ions and hence results in a faster coloration-bleaching time behavior.
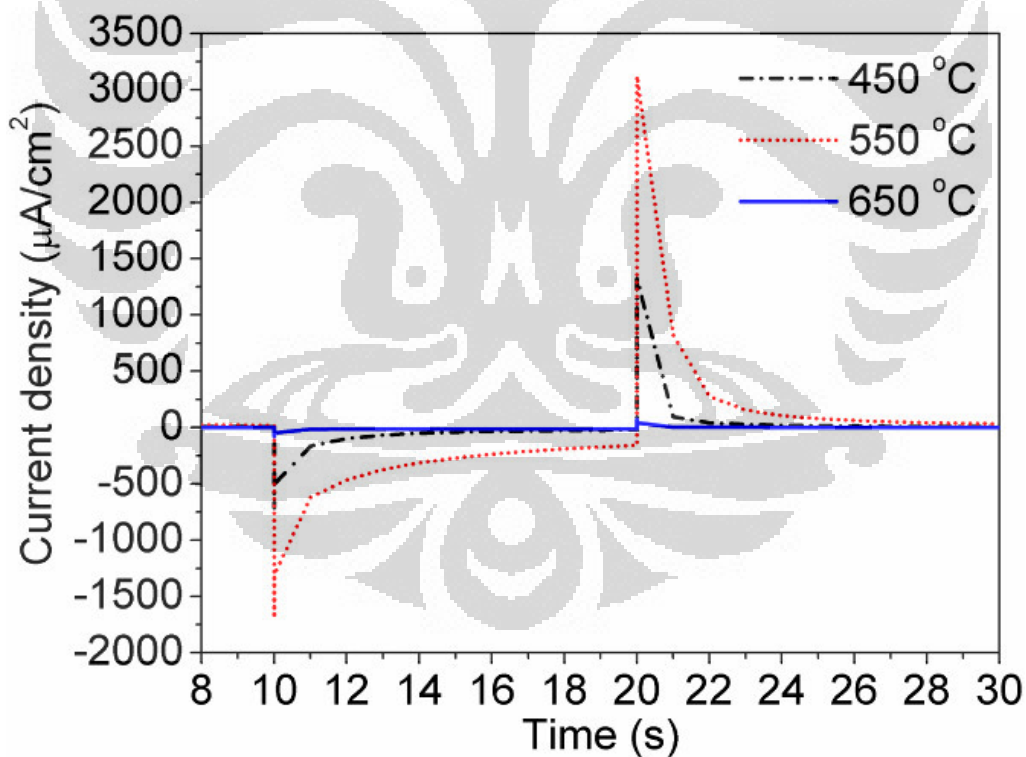
Figure 4-5. Chronoamperometric response (i-t) for thermally oxidized tungsten film at three different heat-treatment temperatures: 450 ^{o}C, 550 ^{o}C, and 650 ^{o}C.

Figure 4-6 shows the chronocoulometry data of thermally oxidized tungsten film with the potential being stepped from -1 to +1 V (Versus SCE) for a step of 10 s. The electrochromic reversibility was calculated as the ratio of deintercalated charge (Q_{di}) to intercalated charge (Q_i), and the results are given in Table 4-2. Samples thermally oxidized at 450 ^{o}C and 550 ^{o}C are easily reversible for lithium ion insertion and extraction, but the reversal of the 650 ^{o}C sample is somewhat inhibited, possibly due to the sample's higher resistance, hence the lithium ion insertion and extraction are hardly reversible. These results are in agreement with [10-11].
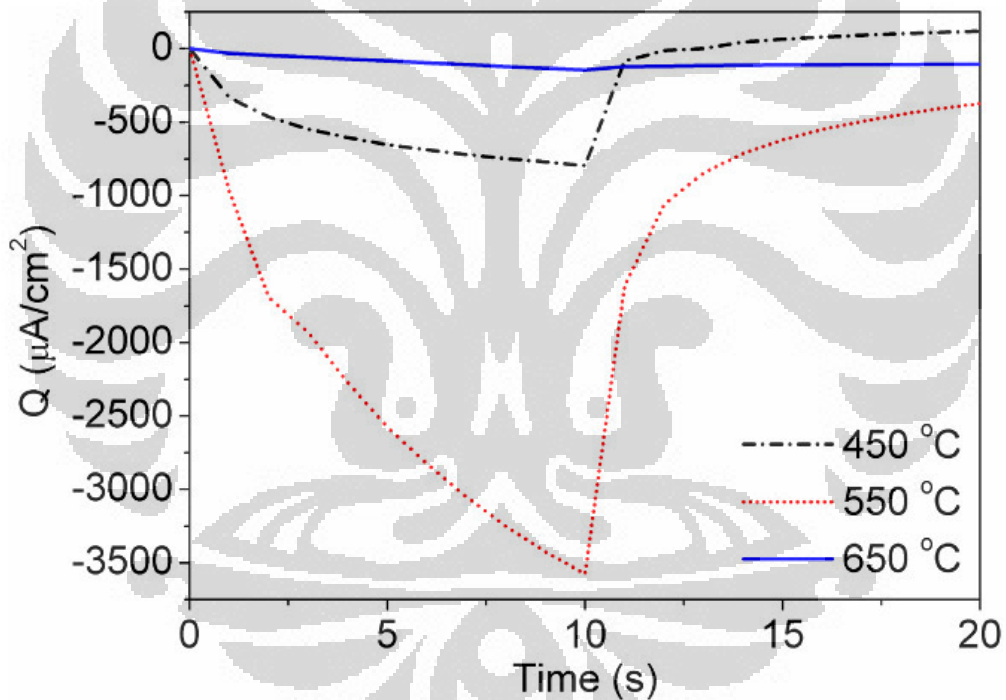
Figure 4-6. Chronocoulometry curve for thermally oxidized tungsten film at three different heat-treatment temperatures: 450 ^{o}C, 550 ^{o}C, and 650 ^{o}C.

4.5 Effect of heat-treatment on the optical transmittance studies

Transmission spectra recorded for all samples in their bleached and colored states are shown in Fig. 4-7. The transmittance difference (ΔT) and the change in optical density (ΔOD) between the bleached and colored states at 630 nm are respectively calculated using relations (3) and (4).

$$\Delta T = \left[\frac{T_b}{T_c}\right]_{\lambda=630} \tag{3}$$

$$\Delta OD = ln\left(\frac{T_b}{T_c}\right)_{\lambda=630} \tag{4}$$

where T_b and T_c are the transmittance of the thermally oxidized tungsten film in its respective bleached and colored states at $\lambda = 630$ nm. It has been observed that increasing the thermal oxidization temperature decreases from 450 ^{o}C to 650 ^{o}C, ΔT and hence ΔOD, at 630 nm from 2.16 to 0.49.

Coloration efficiency (CE) is defined as the change in optical density (ΔOD) per unit of inserted charge and is calculated by relation (5), with results listed in Table 4-3.

$$CE = \frac{(\Delta OD)_{\lambda=630}}{\Delta Q} \tag{5}$$

where ΔQ is the amount of charge intercalated in the sample to cause change in optical density (ΔOD), which was estimated by the curve of current density versus time. The 550 ^{o}C sample has the maximum CE (60.4 cm^2/C), which indicates that the coloration efficiency might be affected by the larger diffusion coefficient, electrochromic reversibility, and electrical conductivity of the film thermally oxidized at 550 ^{o}C. It is important to note that the CE values measured for the thermally oxidized tungsten film at 550 ^{o}C (60.4 cm^2/C) is comparable and possibly improved over state of the art nanostructured tungsten oxides thin films (63.7 cm^2/C) [12].

Table 4-3. Effect of thermal oxidization on coloration efficiency and optical modulation

Heat-treatment condition	T_b (%)	T_c (%)	$(\Delta T)_{\lambda=630 \text{ nm}}$	$(\Delta OD)_{\lambda=630 \text{ nm}}$	ΔQ(C/cm^2)	$CE_{630 \text{ nm}}$ (cm^2/C)
450 ^{o}C	63.4	7.3	56.1	2.16	0.072	30
550 ^{o}C	67.2	13.9	53.3	1.57	0.026	60.4
650 ^{o}C	72.1	44.1	28	0.49	0.078	6.3

The smart windows device with higher coloration efficiency only needs low charge transfer and this also provides better stability. Therefore, the tungsten oxides thin film with heat-treatment temperature at 550 ^{o}C, corresponding to the maximum electrochromic performance, would be further adapted in the commercial application of smart windows.
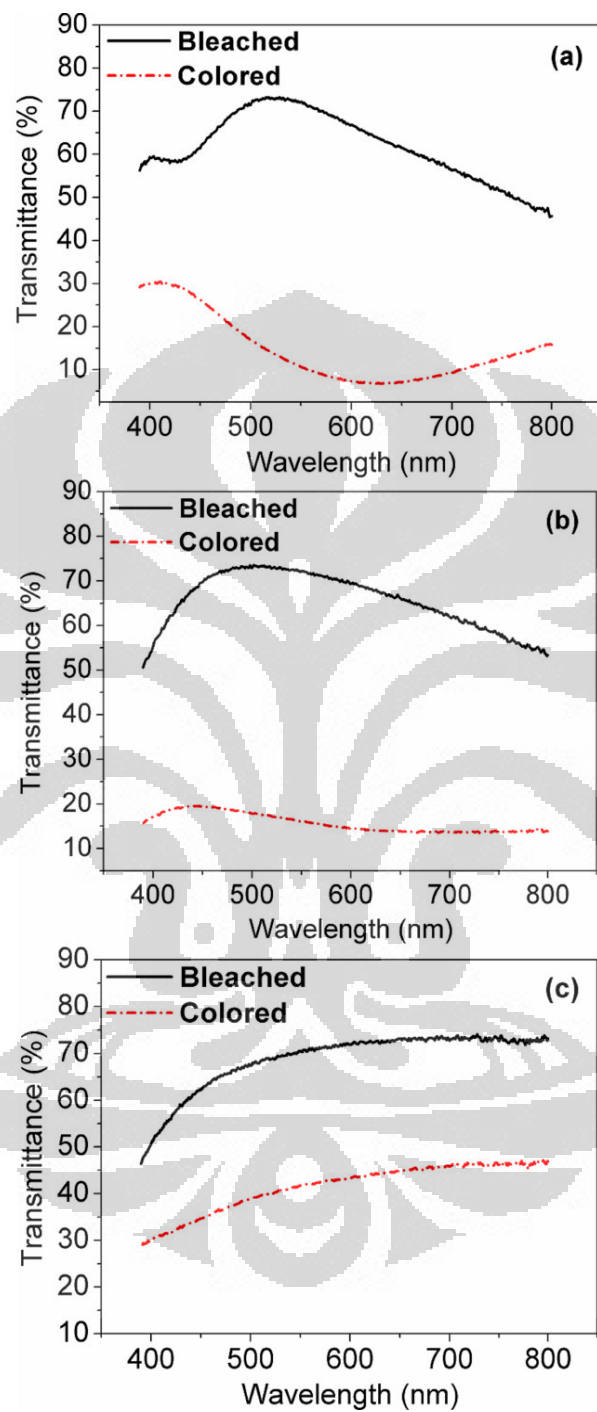
Figure 4-7. Transmission spectra for thermally oxidized tungsten film at (a) 450 ^{o}C, (b) 550 ^{o}C and (c) 650 ^{o}C in its bleached and colored states.

4.6 Conclusion

Tungsten thin films were thermally oxidized to form tungsten oxide films using the heat-treatment technique. The X-ray diffraction (XRD) analysis indicates that a tetragonal WO_3 phase was formed at temperatures below 550 ^oC, and the phase transformed to monoclinic $W_{18}O_{49}$ when the temperature was raised to 650 ^oC. Scanning electron microscopy (SEM) shows that the morphology and structure of the tungsten oxide film could be changed by heat-treatment technique. Electrochromic performance measurements were performed in electrolyte (1 M $LiClO_4$ in PC-water mixtures). The recorded cyclic voltammogram, hence the diffusion coefficient, is maximized in the 550 ^oC ($1.7x10^{-11}$ cm^2/s), followed by 450 ^oC ($5.2x10^{-12}$ cm^2/s) and 650 ^oC ($4.2x10^{-14}$ cm^2/s). The chronoamperometric plots suggest that the response time and the electrochromic reversibility is the best for tetragonal WO_3 films (450 ^oC and 550 ^oC samples). The electrical properties analysis confirmed that the highest electrical conductivity show the superior electrochromic performance, with the maximum coloration efficiency value of 60.4 cm^2/C. Therefore, the tetragonal WO_3 films, with heat-treatment temperature 550 ^oC and 450 ^oC, exhibit good electrochromic properties such as a high diffusion coefficient ($1.7x10^{-11}$ cm^2/s), fast electrochromic response time (coloration time 1.6 s, bleaching time 1.2 s) and high coloration efficiency (60.4 cm^2/C).

Chapter 5

Tungsten Oxide Nanowires for Highly Improved Electrochromic Smart Windows

5.1 Experimental Details

Tungsten films were deposited onto indium tin oxide (ITO) glass substrates by a reactive RF magnetron sputtering system. ITO glass substrates were cut into small pieces with the specific size of 1 cm (width) x 1.5 cm (length). These substrates were ultrasonically cleaned using ethanol and deionized water (Delta Ultrasonic Cleaner; 20 min). The ultrasonic cleaning was followed by nitrogen jet spray to achieve removal of particles from the substrates.

The sputtering system used pure (99.99%) tungsten as a target and pure (99.99%) argon as the sputtering gas with a base chamber pressure of ~3×10^{-5} Torr. Prior to the deposition process, pre-sputtering was performed for about 5 min to clean the target surface. The samples were then generated at an argon flow rate of 25 sccm (standard cubic centimeter per minute) and an RF power of 100 W for 3 minutes. The thickness of the tungsten films were ~150 nm.

The reaction for growth of tungsten oxide nanowires was carried out in a horizontal quartz tube furnace at various heat-treatment temperatures ranging from 400 to 700 ^{o}C. For the first step, the as-deposited tungsten film samples were loaded into a vacuum condition and placed in the middle of a quartz tube furnace. The samples were then heated from 400 to 700 ^{o}C in the total pressure of approximately 50 Torr for 1 hour with a continuous nitrogen flow of 150 sccm. Then, the samples were cooled in the furnace to room temperature. The final step, the annealed samples were oxidized with a continuous O_2 flow of 10 sccm at 450 ^{o}C for 30 min to grow tungsten oxide nanowires.

50

The surface morphology of the tungsten oxide films was visualized by a JEOL JSM-6500F field emission scanning electron microscope (FESEM) at 15 kV. The crystallinity of the samples was characterized by X-ray diffraction (XRD) recorded at a 2θ configuration using a Bruker D8 Discovery X-ray diffractrometer with non-monochromated Cu Kα X-ray radiation (λ= 1.54056 Å). The 2θ investigation region was in the 20°-70° range with a scanning speed of 2 degrees/s. In addition, the electrochemical intercalation and deintercalation of the samples was carried out in a potentiostat controlled by a personal computer in a three electrode cell configuration with 1 M lithium perchlorate ($LiClO_4$) in a propylene carbonate (PC)-water mixture as the electrolytes, a platinum plate as the counter electrode, tungsten oxide as the working electrode and the saturated calomel electrode (SCE) as the reference electrode. A Keithley 237 electrometer was used for the electrical resistance measurement. Optical transmittances spectra were recorded on a JASCO V-560 UV-Vis spectrophotometer. The transmission spectra switch of a tungsten oxide films was examined in the spectral region between 300 and 800 nm by applied coloring/bleaching voltage (- 3.5 V/ +2.0 V).

5.2 Structural Properties Analysis

5.2.1 Structural Properties Analysis of Two-Step Heat Treatment

Tungsten oxide can exhibit different crystal structures, such as cubic and hexagonal WO_3, monoclinic $WO_{2.92}$, and monoclinic $W_{18}O_{49}$. Figure 5-1 shows XRD pattern of the crystal phase transformation of the as-deposited and tungsten oxide films at four different growth temperatures (400 ^{o}C, 500 ^{o}C, 600 ^{o}C, and 700 ^{o}C) with oxidization process. The XRD pattern of the as-deposited tungsten film on ITO-glass substrate (Fig. 5-1a) displays three diffraction peaks at 2θ = 37.5^o, 39.8^o, and 45.5^o, which could be well indexed to a β-W phase (lattice constants: a = 5.05 Å; JCPDS Card 47-1319). These three peaks are assigned to the (200), (210), and (211) crystallographic planes of the β-W phase. Chen et al., showed that, based on the experimental conditions, the lattice parameter of β-W varies from 0.496 to 0.518

51

nm [1]. These reported values are in line with our obtained results. In addition, the diffraction peaks exhibit the broadened peaks of the 2θ region ($33\text{-}46^{\circ}$) which indicates that the crystalline structure of the as-deposited tungsten film coexists with an amorphous phase.

The heat-treatment temperature at 400 $^{\circ}$C (Fig. 5-1b) resulted in the formation of monoclinic $WO_{2.92}$ (lattice constants: a = 11.93 Å, b = 3.820 Å, c = 59.720 Å, β = 98.300°; P2/c; JCPDS Card 30-1387) as indicated by the presence of three diffraction peaks at 2θ = 23.2°, 24.2° and 33.4°, corresponding to the (010), ($\bar{1}$016), and ($\bar{1}$116) lattice planes. Further heat-treatment at 500 $^{\circ}$C and 600 $^{\circ}$C (Figs. 5-1c and d) can be well indexed to be hexagonal WO_3 structure. The heat-treatment at 500 $^{\circ}$C resulted in the formation of hexagonal WO_3 with cell constants: a = 7.324 Å, c = 7.662 Å; P63/mcm; JCPDS Card 85-2460. On the other hand, the heat-treatment at 600 $^{\circ}$C resulted in the formation of hexagonal WO_3 with lattice constants: a = 7.298 Å, c = 3.899 Å; P6/mmm; JCPDS Card 33-1387. The detectable difference between the two samples are the stronger intensity and narrowing of the diffraction peaks at 2θ = ~23° and ~27°, and also ITO peaks. Finally, a heat-treatment temperature at 700 $^{\circ}$C (Fig. 5-1d) results in the disappearance of the hexagonal WO_3 phase peaks and the emergence of new peaks at 2θ = 29.2°, 23.4°, and 27.9°. These peaks are assigned to the (130), (001), and (200) lattice planes of the monoclinic W_3O_8 phase (cell constants: a = 6.386 Å, b = 10.43 Å, c = 3.800 Å; C222; JCPDS Card 81-2262). Multiple sharp peaks appeared when the temperature is increased to 600 and 700 $^{\circ}$C. This phenomenon was identified as a residual stress in the tungsten film at higher temperatures [2]. However, the 700 $^{\circ}$C sample also results in the phase transition from hexagonal WO_3 to orthorhombic W_3O_8. Tungsten oxide crystal phase at four different heat-treatment temperatures are described in Table 5-1.

Figure 5-2 shows the SEM images for the surface morphology of the tungsten oxide films at four different heat-treatment temperatures. As shown in Fig. 5-2a, the heat-treatment temperature at 400 $^{\circ}$C has a smooth surface and no grains. However, when the temperature

was increased to 500 °C (Fig. 5-2b), nanowires with length of 212 nm are clearly seen. The growth of the tungsten oxide nanowires at the 500 °C sample appears similar to the tungsten oxide nanostrucuture morphology reported by Seongho et al [3]. The surface morphology of tungsten oxide nanowires coalesced to form irregular block-like morphology with length of 250-700 nm when the growth temperature increased up to 600 °C (Fig. 5-2c). The size increases at the 600 °C sample possibly due to the growth and agglomeration of the tungsten oxide nanowires at the higher temperature [4]. Finally, a heat-treatment temperature at 700 °C (Fig. 5-2d) result tungsten film of nano grains with spherical grains diameters of 60-130 nm. Tungsten oxide surface morphology at four different heat-treatment temperatures are described in Table 5-1.
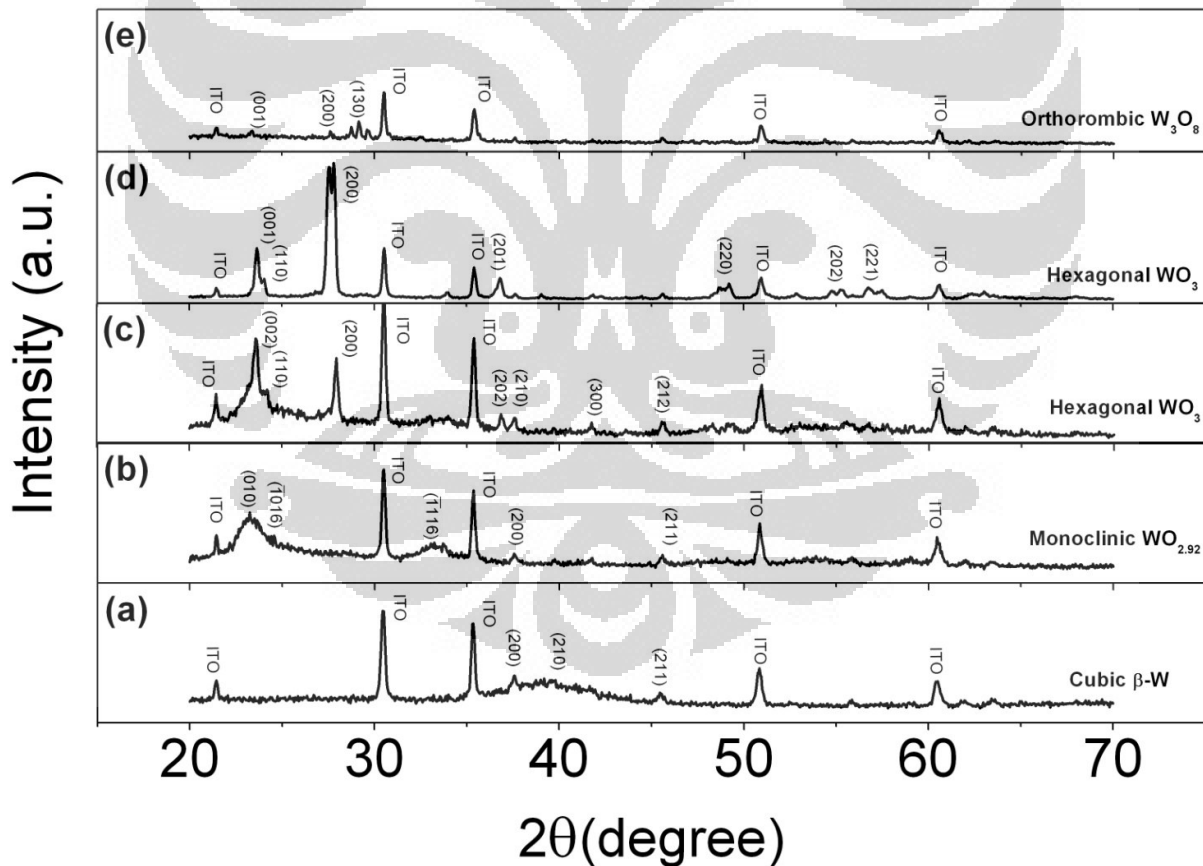
Figure 5-1. XRD patterns of (a) as-deposited and tungsten oxide at four different growth temperatures: (b) 400 °C, (c) 500 °C, (d) 600 °C, and (e) 700 °C, with oxidization process.

53
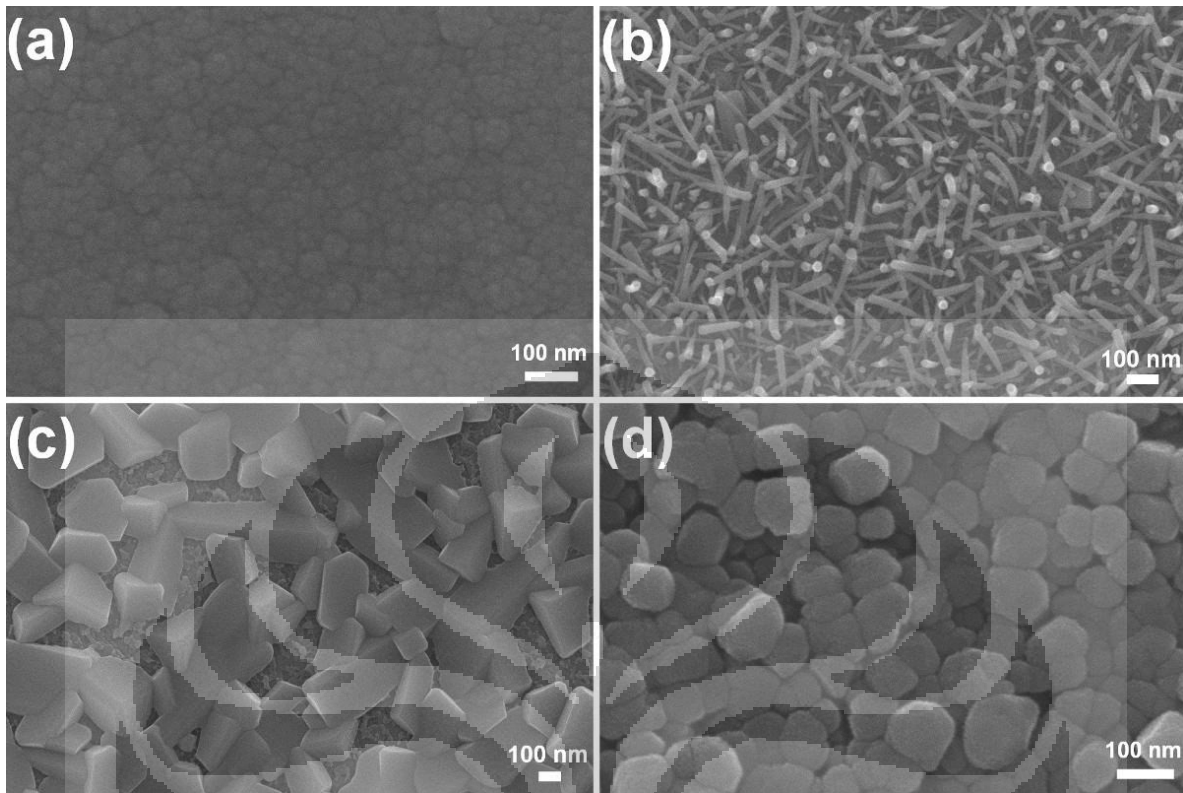
Figure 5-2. SEM image of tungsten oxide at four different growth temperatures: (a) 400 ^{o}C, (b) 500 ^{o}C, (c) 600 ^{o}C and (d) 700 ^{o}C, with oxidization process.

Table 5-1. Tungsten oxide surface morphology and crystal phase at four different heat-treatment temperatures (400 ^{o}C, 500 ^{o}C, 600 ^{o}C, and 700 ^{o}C) with oxidization process.

Thermal condition	Surface morphology	Crystal phase (Crystal structure; lattice constants; space groups)
400 ^{o}C	Smooth crystalline surface and no grains	Monoclinic $WO_{2.92}$; a = 11.93 Å, b = 3.820 Å, c = 59.720 Å, β = 98.300^{o}; P2/c
500 ^{o}C	Nanowires (212 nm length)	Hexagonal WO_3; a = 7.324 Å, c = 7.662 Å; P63/mcm
600 ^{o}C	Irregular block-like (250-700 nm length)	Hexagonal WO_3; a = 7.298 Å, c = 3.899 Å; P6/mmm
700 ^{o}C	Film of nano grains with spherical grains (60-130 nm)	Orthorhombic W_3O_8; a = 6.386 Å, b = 10.43 Å, c = 3.800 Å; C222

54

5.2.2 Oxidization Effect on the Structural Properties of Two-Step Heat Treatment

To investigate oxidization effect on the structural properties of the two-step heat treatment, we deposited under the same conditions as those given in the Sec. 5.1 and annealed a sputtered W film at 500 °C and 600 °C for 1 hour without oxidization. From this investigated, we try to examine what is the effect of oxidation on the structural properties tungsten oxide film. Figure 5-3 shows (a) SEM images and (b) XRD pattern of the surface morphology of W films before and after oxidization of tungsten oxide 500 °C growth temperatures. As seen in Fig. 5-3a, surface morphology of tungsten oxide film after annealed at 500 °C for 1 hour without oxidization show nanowires structure with length of 65 nm. The length of nanowires increases after oxidization process, from 65 nm to 212 nm. Moveover, the density of tungsten oxide nanowires after oxidation is higher than before oxidization. The XRD pattern indicated that WO_{3-x} tungsten oxide structure presence on the before and after oxidation samples. The only detectable difference between the two samples is the stronger intensity of the WO_3 at the diffraction peak at $2\theta = \sim 27°$ when the samples oxidized after annealing. This suggests that the oxidized sample has better crystallinity than without oxidization. These results indicate that the oxidization process must be important for growing tungsten oxide nanowires with long nanowire formation and good crystallinity.

Furthermore, Fig. 5-4 shows (a) SEM images and (b) XRD pattern of the surface morphology of W films before and after oxidization of tungsten oxide 600 °C growth temperatures. As seen in Fig. 5-4a, surface morphology of tungsten oxide film after annealed at 600 °C for 1 hour without oxidization is not uniform of irregular block-like tungsten oxide. Moreover, the density and uniformity of irregular block-like tungsten oxide increase after the oxidation process. The XRD pattern indicated that WO_{3-x} tungsten oxide structure presence on the before and after oxidation samples. The difference between the two samples is the stronger intensity of the WO_3 at the diffraction peak at $2\theta = \sim 27°$ when the samples oxidized after

55

annealing. This suggests that the oxidized sample has better crystallinity than without oxidization. These results indicate that the oxidization process must be important for better crystallinity of tungsten oxide structure.

5.3 Electrical Property Analysis

Figure 5-5 shows electrical measurement of the tungsten oxide at four different heat-treatment temperatures. This figure shows that the best conductivity is in the 500 $^{\circ}$C growth temperature. When the temperature raised up to 600 $^{\circ}$C, there was a significantly decrease of conductivity, which may be due to the interface of tungsten oxide–ITO could be modified by making the electrode very resistive when the higher temperature caused the ITO tend to decompose [5]. According to Alam et al. [6] with increasing annealing temperature up to 500 $^{\circ}$C, the ITO thin films would perform higher conductivity. Moreover, as observe in the SEM, the tungsten oxide in the 500 $^{\circ}$C heat-treatment temperature exhibit the nanowires structure. Thus, the increase in conductivity in the 500 $^{\circ}$C heat-treatment temperature might be the reason that the nanowires structure leading to evolution of tungsten–oxygen networks.

Figure 5-3. (a) SEM image of the tungsten oxide film at growth temperatures 500 °C with

oxidization process. Inset is the image of the tungsten oxide film sample before oxidization. (b)

XRD pattern of the tungsten oxide film at growth temperatures 500 °C before and after oxidization.
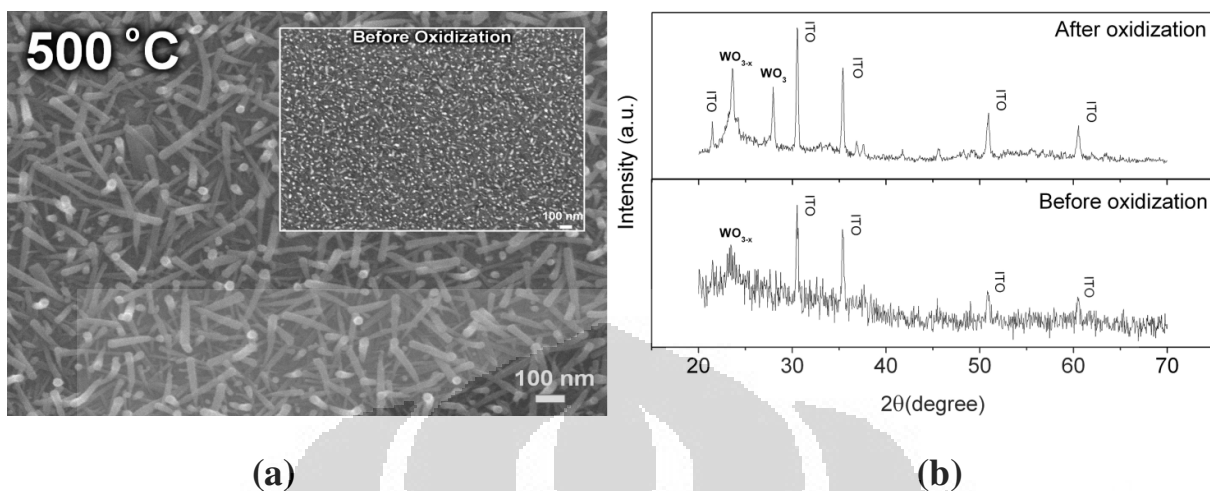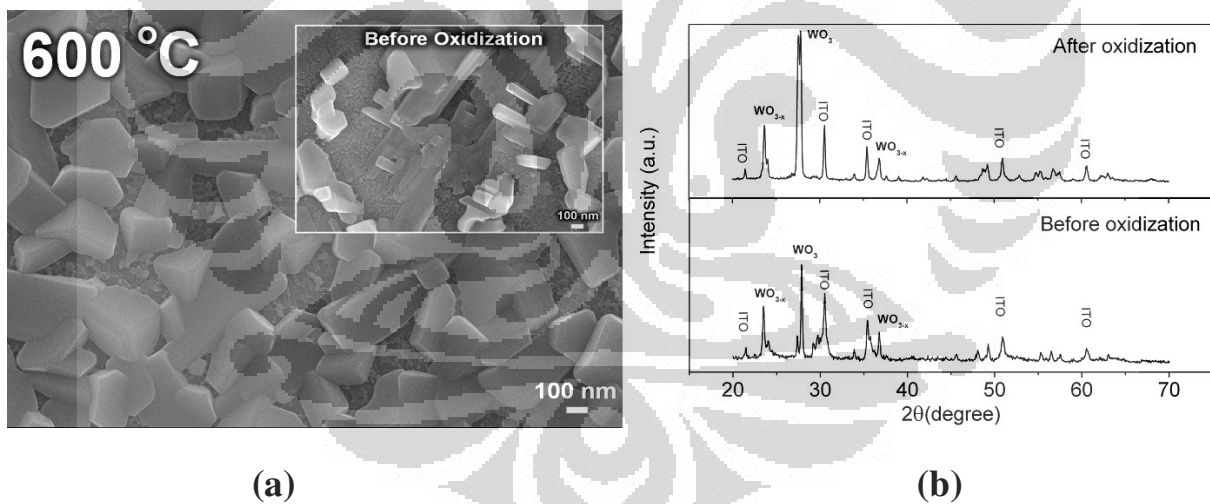

Figure 5-4. (a) SEM image of the tungsten oxide film at growth temperatures 600 °C with

oxidization process. Inset is the image of the tungsten oxide film sample before oxidization. (b)

XRD pattern of the tungsten oxide film at growth temperatures 600 °C before and after oxidization.

57
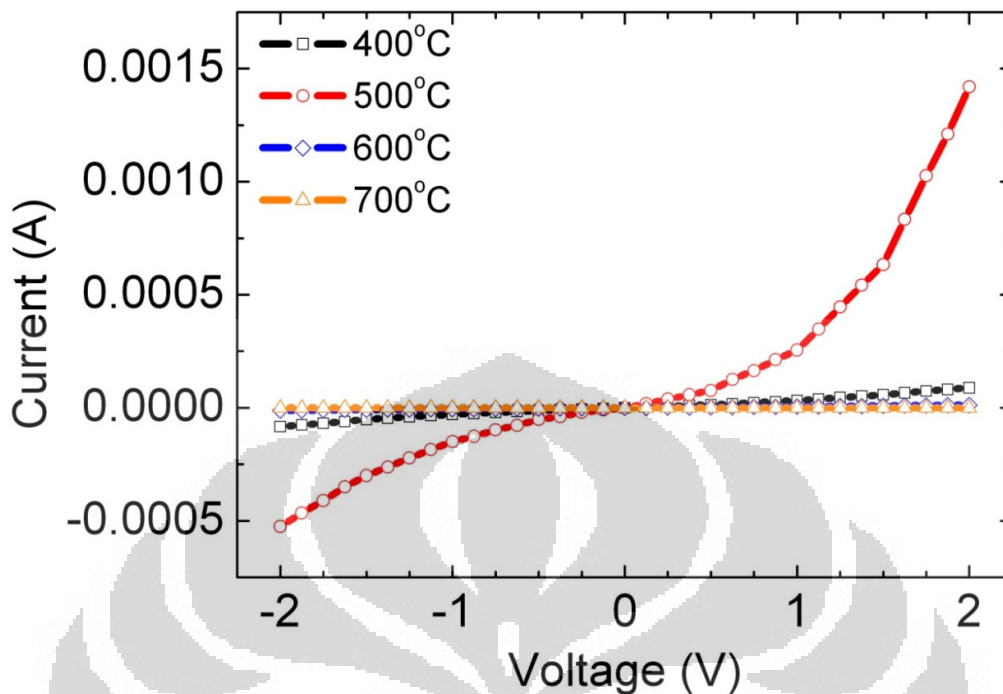
Figure 5-5. I-V measurements of tungsten oxide at four different growth temperatures (400 °C, 500 °C, 600 °C, and 700 °C) with oxidization process.

5.4 Electrochromic Properties Analysis

Figure 5-6 shows cyclic voltammograms recorded at a 100 mV/s scanning rate with a linear potential sweep of -1 to 1 V (Versus SCE) for tungsten oxide at four different heat-treatment temperatures. The cathodic peak current (I_{pc}), anodic peak current (I_{pa}), cathodic peak voltage (V_{pc}), and anodic peak voltage (V_{pa}) values are given in Table 5-2. The current recorded is due to a cation intercalation/deintercalation according to the reaction

$$WO_3(bleach) + xLi^+ + xe^- \leftrightarrow Li_xWO_3(blue) \tag{1}$$

where Li$^+$ is ion in the lithium perchlorate organic solution. The integrated cathodic-current density equates to the amount of lithium ions intercalated to form a tungsten bronze.

58

Figure 5-6 shows that the voltammogram area, hence the charge storage capacity, is maximized in the 500 $^{\circ}$C sample (tungsten oxide nanowires structure), followed by 400 $^{\circ}$C, 600 $^{\circ}$C and 700 $^{\circ}$C samples. The absolute value of peak current density is an indication of the electrochemical activity of the working electrode [7]. The results presented in Table 5-2 show that the value of the peak current (I_{pc} and I_{pa}) is highest in tungsten oxide nanowires structure.

Furthermore, the insertion efficiencies for these samples are determined by diffusion coefficients calculated using the well-known Randles-Servcik equation [8]

$$D^{1/2} = \frac{i_p}{2.72 \times 10^5 \times n^{3/2} \times A \times C_o \times v^{1/2}} \tag{2}$$

where i_p is the cathodic peak current density, $n = 1$ is the number of electrons, A is area of the film, Co is the electrolyte concentration (1 M), and v is the scan rate. Calculated values are given in Table 5-2. The diffusion coefficient of 2×10^{-9} cm^2/s for the 500 $^{\circ}$C sample (tungsten oxide nanowires structure) is the largest, closely followed by the diffusion coefficient of 1.3×10^{-10} cm^2/s and 6.7×10^{-11} cm^2/s for the 400 $^{\circ}$C and 600 $^{\circ}$C samples, respectively. The lowest diffusion coefficient of 5×10^{-15} cm^2/s is found in the 700 $^{\circ}$C sample, which is a natural consequence of its peak current density. Therefore, the heat-treatment at 500 $^{\circ}$C, which exhibit tungsten oxide nanowires structure, has the greatest electrochemical activity and diffusion coefficient, may be due to short diffusion path of Li$^+$ on the tungsten oxide nanowires [11] and the highest conductivity [12] which allows for the easy transport of Li$^+$ ions across the film and thus enhances the peak current.

59
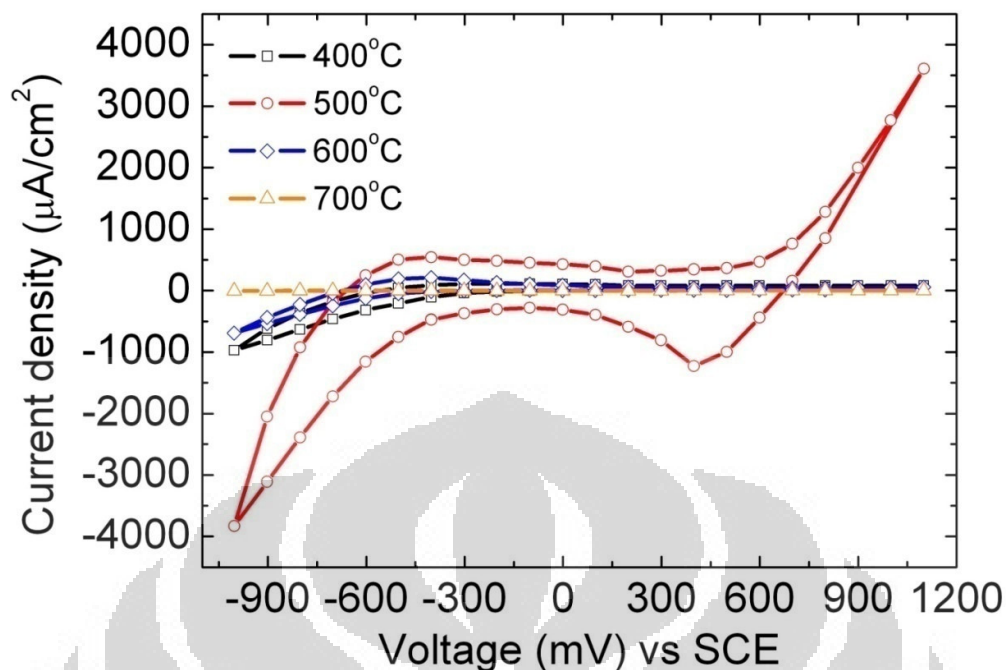
Figure 5-6. Cyclic voltammograms spectra for tungsten oxide at four different growth temperatures (400 ^{o}C, 500 ^{o}C, 600 ^{o}C, and 700 ^{o}C) with oxidization process.

Table 5-2. Electrochromic performance of tungsten oxide at four different growth temperatures (400 ^{o}C, 500 ^{o}C, 600 ^{o}C, and 700 ^{o}C) with oxidization process.

Heat-treatment condition	I_{pc} (μA/cm^2)	I_{pa} (μA/cm^2)	E_{pc} (mV)	E_{pa} (mV)	Diffusion coefficient (cm^2/s)
400 ^{o}C	972	112	1003	204	1.3x10^{-10}
500 ^{o}C	3826	3607	1002	1105	2x10^{-9}
600 ^{o}C	691	213	1002	402	6.7x10^{-11}
700 ^{o}C	6	2	1002	202	5x10^{-15}

Figure 5-7 shows typical chronoamperometric (CA) traces recorded during coloration and bleaching of the tungsten oxide at four different heat-treatment temperatures. During the experiment, CA cycling was performed on the tungsten oxide between +1 and -1 V (versus SCE).

60

The voltage was stepped from 0 to -1 V for 10 s (coloration) and then reversed to +1 V for the next 10 s (bleaching). The CA technique was used to measure the response time for the tungsten oxide. Response times for coloration (t_c) and bleaching (t_b) were calculated from current time transients and the results are given in Table 5-3. The plots suggest that the response time are the fastest in the 500 ^{o}C sample (coloration time 1.7 s, bleaching time 1.1 s), which exhibit the nanowires structure possibly due to decrease the diffusion distance of the Li$^+$ ions by tungsten oxide nanowires structure $[\, l \approx \sqrt{Dt} : l = diffusion\ distance, t = response\ time\,]$ [11,13] and hence results in a faster coloration-bleaching time behavior.

Figure 5-8 shows the chronocoulometry data of tungsten oxide with the potential being stepped from -1 to +1 V (Versus SCE) for a step of 10 s. The electrochromic reversibility was calculated as the ratio of deintercalated charge (Q_{di}) to intercalated charge (Q_i), and the results are given in Table 5-3. Heat-treatment temperatures samples at 400 ^{o}C, 500 ^{o}C, and 600 ^{o}C are easily reversible for lithium ion insertion and extraction, but the reversal of the 700 ^{o}C sample is somewhat inhibited, possibly due to the sample's higher resistance, hence the lithium ion insertion and extraction are hardly reversible. These results are in agreement with [9-10].

Figure 5-7. Chronoamperometric response (i-t) for the tungsten oxide at four different growth temperatures (400 ^{o}C, 500 ^{o}C, 600 ^{o}C, and 700 ^{o}C) with oxidization process.
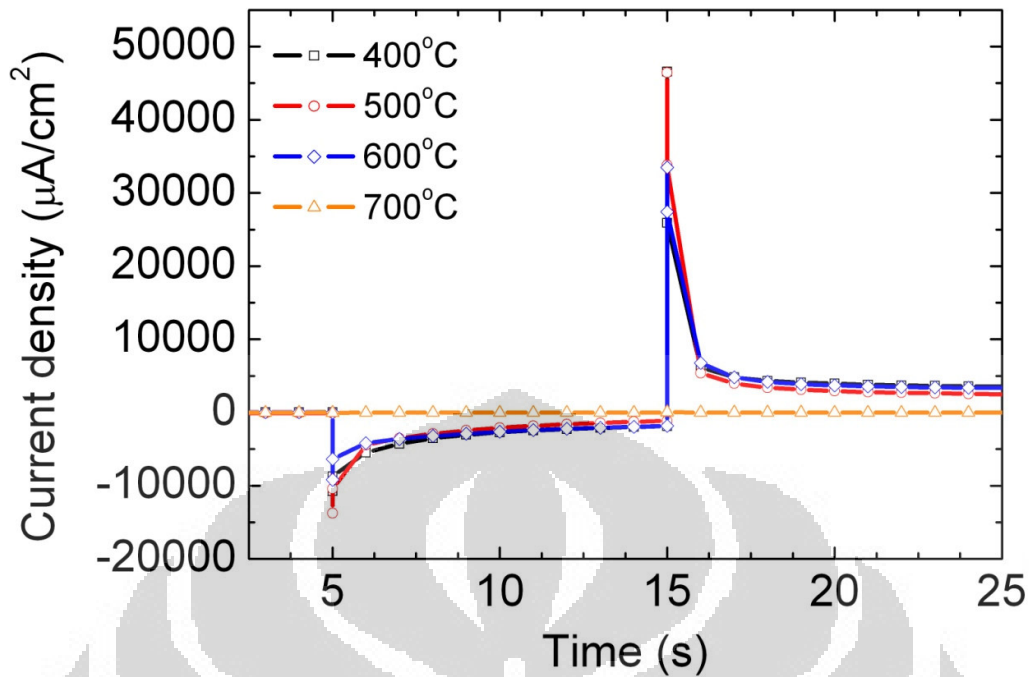

Figure 5-8. Chronocoulometry curve for tungsten oxide at four different growth temperatures (400 ^{o}C, 500 ^{o}C, 600 ^{o}C, and 700 ^{o}C) with oxidization process.
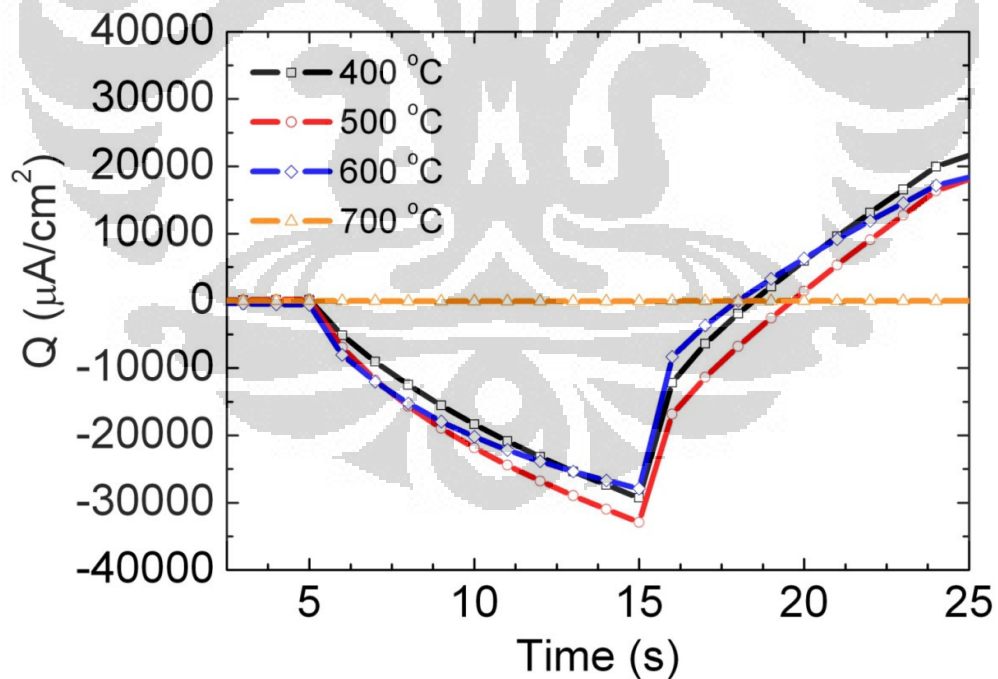
Table 5-3. Chronoamperometry and chronocoulometry measurement of tungsten oxide at four different growth temperatures (400 °C, 500 °C, 600 °C, and 700 °C) with oxidization process.

Heat-treatment condition	Response time		Q_i (μC/cm^2)	Q_{di} (μC/cm^2)	$(Q_i - Q_{di})$ (μC/cm^2)	Reversibility (%)
	t_c (s)	t_b (s)				
400 °C	2.5	1.3	29260	12160	17100	41.7
500 °C	1.7	1.1	32910	16840	16070	51.2
600 °C	3	1.3	27900	8320	19580	29.8
700 °C	-	-	-	-	-	-

5.5 Optical Transmittance Studies

Figure 5-9 shows the transmission spectra for all samples in their bleached and colored states. The transmittance difference (ΔT) and the change in optical density (ΔOD) between the bleached and colored states at 500 nm are respectively calculated using relations (3) and (4).

$$\Delta T = \left[\frac{T_b}{T_c}\right]_{\lambda=500} \tag{3}$$

$$\Delta OD = ln\left(\frac{T_b}{T_c}\right)_{\lambda=500} \tag{4}$$

where T_b and T_c are the transmittance of tungsten oxide in its respective bleached and colored states at $\lambda = 500$ nm.

Coloration efficiency (*CE*) is defined as the change in optical density (ΔOD) per unit of inserted charge and is calculated by relation (5), with results listed in Table 5-4.

$$CE = \frac{(\Delta OD)_{\lambda=500}}{\Delta Q} \tag{5}$$

where ΔQ is the amount of charge intercalated in the sample to cause change in optical density (ΔOD), which was estimated by integrating the area under the curve of current density versus time. The nanowires structure in the 500 ^{o}C heat-treatment temperature has the maximum CE (67.4 cm^2/C), which indicates that the coloration efficiency might be affected by the morphology structure, electrical conductivity, and larger diffusion coefficient.

Table 5-5 shows the response time and the coloration efficiency of the nanowires reported by other researchers. Our work exhibit faster response time and higher coloration efficiency than that reported earlier by Liao et al. [5], Yoo et al. [11], and Shim et al [12], for nanowires WO$_3$ films. The electrochromic smart windows with higher coloration efficiency only need low charge transfer and this also provides better stability. Therefore, the tungsten oxides nanowire prepared by heat-treatment technique at 500 ^{o}C, corresponding to the maximum electrochromic performance, would be further adopted in the commercial application of smart windows.

Table 5-4. Coloration efficiency and optical modulation of tungsten oxide at four different growth temperatures (400 ^{o}C, 500 ^{o}C, 600 ^{o}C, and 700 ^{o}C) with oxidization process.

Heat-treatment condition	T_b (%)	T_c (%)	$(\Delta T)_{\lambda=500\,nm}$	$(\Delta OD)_{\lambda=500\,nm}$	ΔQ(C/cm^2)	$CE_{500\,nm}$ (cm^2/C)
400 ^{o}C	41.2	13.2	28	1.14	0.043	26.51
500 ^{o}C	60.4	9.8	50.6	1.82	0.027	67.41
600 ^{o}C	31.9	15	16.9	0.76	0.059	12.88
700 ^{o}C	86.2	84.7	1.5	0.02	-	-
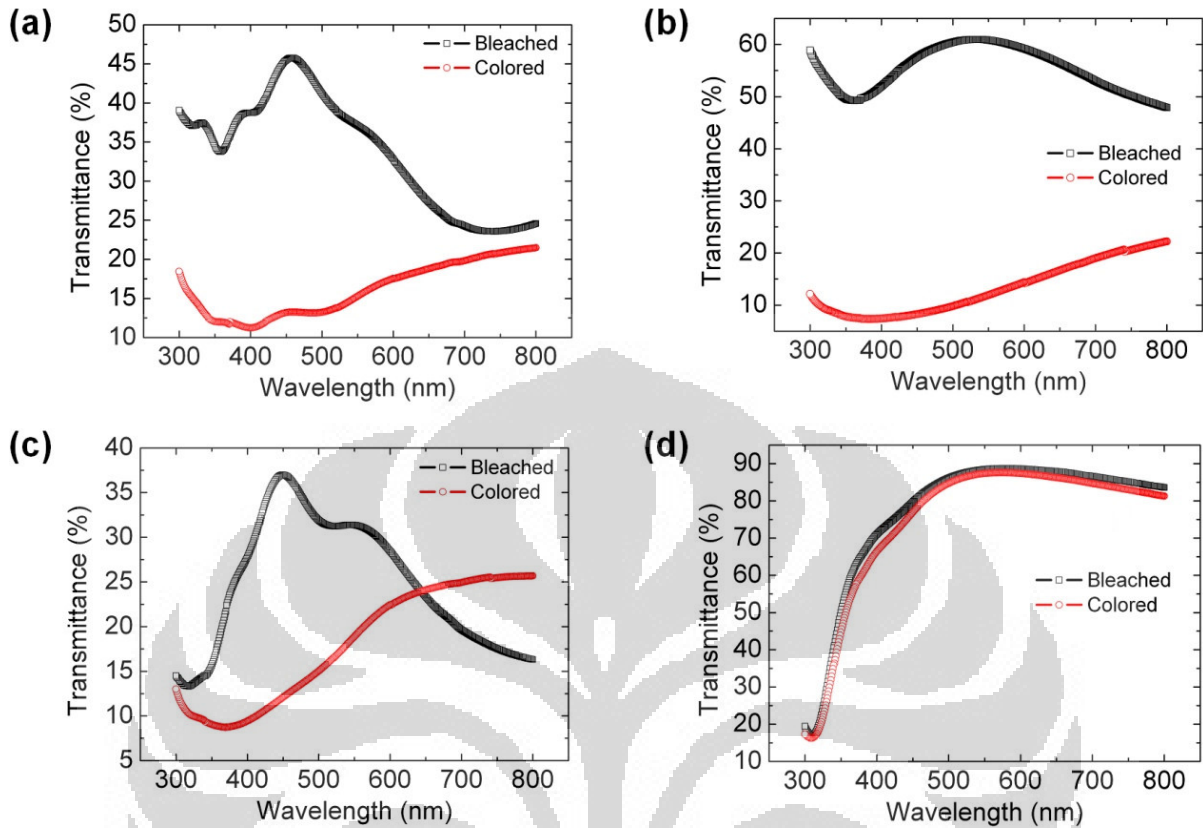
Figure 5-9. Transmission spectra for tungsten oxide at four different growth temperatures: (a) 400 ^{o}C, (b) 500 ^{o}C, (c) 600 ^{o}C, and (d) 700 ^{o}C in its bleached and colored states.

Table 5-5. The response time and the coloration efficiency of the tungsten oxide nanowires

Reference	Diffusion coefficient (cm^2/s)	Response time		Coloration efficiency (cm^2/C)	Transmittance difference [ΔT %]	Synthesis of tungsten oxide	Morphology of tungsten oxide
		t_c (s)	t_b (s)				
Liao et al. [5]	-	3.0	1.5	61.3	64.8	Thermal evaporation	Nanowires
Yoo et al. [11]	1.7×10^{-11}	3.5	1.1	55	-	Solvothermal	Nanowires Bundles
Shim et al. [12]	-	4.2	1.0	56	64.8	Electrospinning	Nanowires
Our Work	2x10^{-9}	1.7	1.1	67.41	50.6	Heat-treatment	Nanowires

65

5.6 Conclusion

Tungsten oxide nanowires were prepared on a tungsten film (W)/ITO-glass substrate at 500 ^{o}C for electrochromic devices using the heat-treatment technique. The X-ray diffraction (XRD) analysis indicates that a cubic β-W phase at as-deposited tungsten film on ITO-glass substrate, a monoclinic $WO_{2.92}$ in the 400 ^{o}C heat-treatment temperature, a hexagonal WO_3 phase was formed at temperatures of 500 ^{o}C and 600 ^{o}C; and the phase transformed to orthorhombic W_3O_8 when the temperature was raised to 700 ^{o}C. Scanning electron microscopy (SEM) shows that the morphology and structure of the tungsten oxide nanowires exhibit in the 500 ^{o}C heat-treatment temperature. Electrochromic measurements were performed in electrolyte (1 M $LiClO_4$ in PC-water mixtures). Electrical conductivity of tungsten oxide and the corresponding electrochromic performance is the best in the 500 ^{o}C heat-treatment temperature. The recorded cyclic voltammogram, hence the diffusion coefficient, is maximized in the 500 ^{o}C (2×10^{-9} cm^2/s), followed by 400 ^{o}C (1.3×10^{-10} cm^2/s), 600 ^{o}C (6.7×10^{-11} cm^2/s), and 700 ^{o}C (5×10^{-15} cm^2/s) heat-treatment temperature. The chronoamperometric plots suggest that the response time are the fastest in the 500 ^{o}C sample (coloration time 1.7 s, bleaching time 1.1 s), which exhibit the nanowires structure. Furthermore, tungsten oxide nanowires structure prepared by the heat-treatment technique shows the maximum coloration efficiency of 67.41 cm^2/C.

Chapter 6

# Conclusion and Future Works

6.1. Conclusion

In this study, tungsten oxide was successfully synthesized (not only thin film structure, but also nanowires structure) on ITO-glass substrate. Thus far, growing of tungsten oxide thin film or nanowires structure on a supporting substrate (ITO-glass substrate) is challenging yet essential for tuning the electrochromic smart windows performance. The resulting of tetragonal WO_3 thin film, with heat-treatment temperature 550 ^{o}C and 450 ^{o}C, exhibit good electrochromic properties such as a high diffusion coefficient (1.7×10^{-11} cm^2/s), fast electrochromic response time (coloration time 1.6 s, bleaching time 1.2 s), and high coloration efficiency (60.4 cm^2/C).

Furthermore, tungsten oxide nanowires shows excellent electrochromic properties such as a high diffusion coefficient (2×10^{-9} cm^2/s), fast electrochromic response time (coloration time 1.7 s, bleaching time 1.1 s), and high coloration efficiency (67.41 cm^2/C). Therefore, the tungsten oxides nanowires prepared by heat-treatment temperature at 500 ^{o}C, corresponding to the maximum electrochromic performance, would be further adapted in the commercial application of smart windows.

6.2 Future Works

In the future work, we should conduct some analysis in the 450 ^{o}C and 550 ^{o}C by heat-treatment technique to make sure that the tungsten oxides nanowires in the 500 ^{o}C is the best electrochromic properties prepared by heat-treatment technique.

Furthermore, we could do further studies for electrochromic durability and stability of tungsten oxide nanowires based smart windows. Since smart windows are usually intended for use everyday, deterioration of smart windows is best gauged by eye and with the same illumination, environment and cell driving conditions, which would be employed during normal operation.
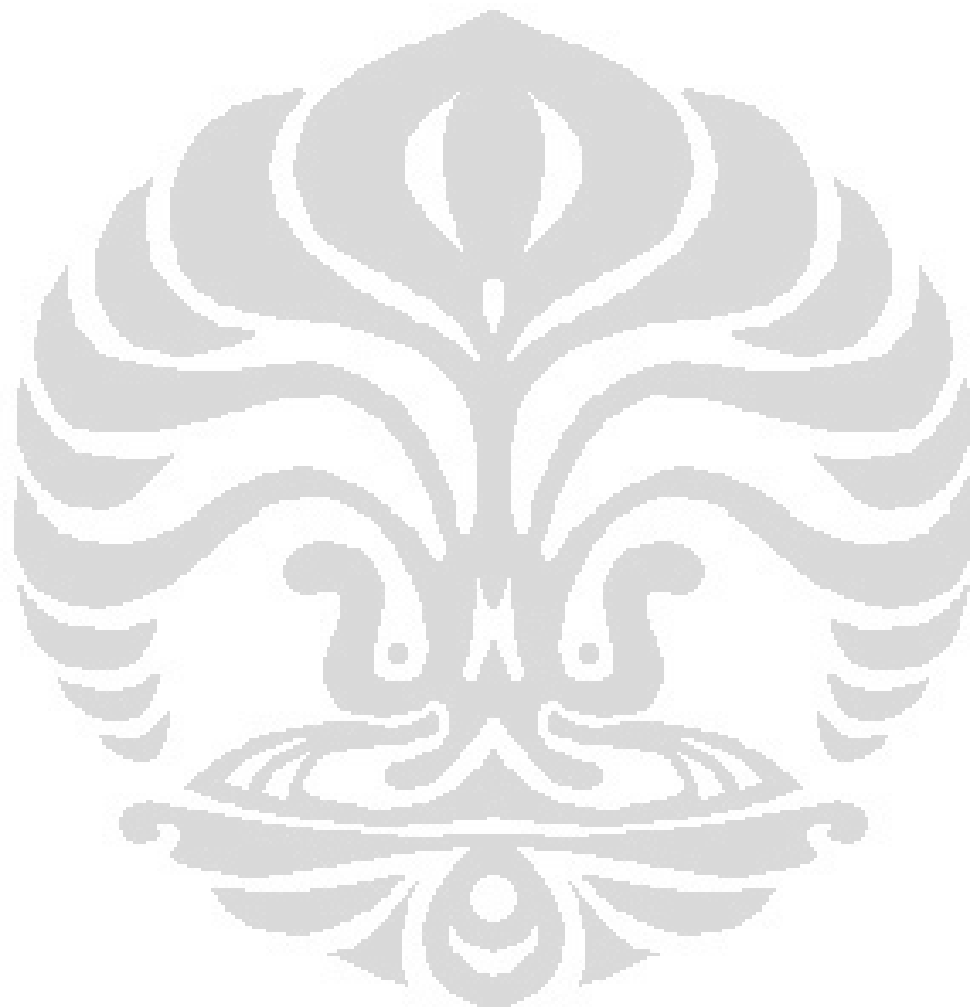
References

Chapter 1

[1]   H. Chhina, S. Campbell, and O. Kesler, J. Electrochem. Soc., 154 (2007) B533.

[2]   A. Ponzonia, V. Russo, A. Bailini, C. S. Casari, M. Ferroni, A. Li Bassi, A. Migliori, V. Morandi, L. Ortolani, G. Sberveglieri, and C. E. Bottani, Sens. Actuators B, 153 (2011) 340.

[3]   J. Zhou, L. Gong, S. Z. Deng, J. Chen, J. C. She, and N. S. Xu, Applied Physics Letters, 87 (2005) 223108(1).

[4]   P. R. Somani and S. Radhakrish, Chemistry and Physics, 77 (2002) 117.

[5]   S. Balaji, Y. Djaoued, A. S. Albert, R. Z. Ferguson, and R. Bruning, Chem. Mater., 21 (2009) 1381.

[6]   M. Z. Najdoski and T. Todorovski, Materials Chemistry and Physics, 104 (2007) 483.

[7]   C. G. Granqvist, Handbook of Inorganic Electrochromic Materials. 1995, New York: Elsevier.

[8]   P. M. S. Monk, R. J. Mortimer, and D. R. Rosseinsky, Electrochromism and Electrochromic Devices. 2007, United Kingdom: Cambridge University Press.

[9]   K. Bange, Sol. Energy Mater. Sol. Cells, 58 (1999) 1.

[10] C. G. Granqvist, Sol. Energy Mater. Sol. Cells, 60 (2000) 201.

[11] C. G. Granqvist, A. Azens, A. L. Kullman, G. A. Niklasson, D. Ronnow, M. S. Mattsson, M. Veszelei, and G. Vaivars, Solar Energy, 63 (1998) 199.

[12] R. Baetens, B. P. Jelle, and A. Gustavsen, Sol. Energy Mater. Sol. Cells, 94 (2010) 87.

[13] A. Azens and C. Granqvist, J. Sol. State Elec. Chem., 94 (2003) 64.

[14] Granqvist, C. G. Sol. Energy Mater. Sol. Cells., 92 (2008) 203.

[15] M. Deepa, A. G. Joshi, A. K. Srivastava, S. M. Shivaprasad, and S. A. Agnihotry, J. Electrochem. Soc., 153 (2006) C365.

[16] Y. Suna, C. J. Murphy, K. R. Reyes-Gil, E. A. Reyes-Garcia, J. M. Thornton, N. A. Morris, and D. Raftery, International Journal of Hydrogen Energy, 34 (2009) 8476.

[17] M. Giannoulia and G. Leftheriotis, Sol. Energy Mater. Sol. Cells, 95 (2011) 1932.

[18] C. Lemire and D. B. B. Lollman, A. Al Mohammad, E. Gilet, and K. Aguir, Sens. Actuators B, 84 (2002) 43.

[19] K. M. Karuppasamy and A. Subrahmanyam, Sol. Energy Mater. Sol. Cells, 92 (2008) 1322.

[20] M. Filipescu, S. Orlando, V. Russo, A. Lamperti, A. Purice, A. Moldovan, and M. Dinescu, Appl. Surf. Sci., 253 (2007) 8258.

[21] R. Sohal, C. Walczyka, P. Zaumseila, D. Wolanskya, A. Foxa, B. Tillacka, H. J. Müssiga, and T. Schroeder, Thin Solid Films, 517 (2009) 4534.

[22] S. Balaji, Y. Djaouned, A. S. Albert, R. Brüning, N. Beaudoin, and J. Robichaud, J. Mater. Chem., 21 (2011) 3940.

[23] X. Sun, Z. Liu, and H. Cao, J. Alloy. Compd., 504S (2010) S418.

[24] X. Sun, H. Cao, Z. Liu, and J. Li, Appl. Surf. Sci., 255 (2009) 8629.

[25] D. Gogova, L. K. Thomas, and B. Camin, Thin Solid Films, 517 (2009) 3326.

[26] E. Ozkan, S. H. Lee, C. E. Tracy, F. Z. Tepehan, J. R. Pitts, and S. K. Deb, Solid State Ionics, 149 (2002) 139.

[27] M. Deepa, A. K. Srivastava, K. N. Sood, and S. A. Agnihotry, Nanotechnology, 17 (2006) 2625.

[28] S. J. Yoo, J. W. Lim, Y. E. Sung, Y. H. Jung, H. G. Choi, and D. K. Kim, Applied Physics Letters, 90 (2007) 173126 (1).

[29] S. J. Yoo, Y. H. Jung, J. W. Lim, H. G. Choi, D. K. Kim, and Y. E. Sung, Sol. Energy Mater. Sol. Cells, 92 (2008) 179.

[30] G. Gu, B. Zeng, W. Q. Han, S. Roth, and J. Liu, Nano Letters, 2 (2002) 849.

[31] C. Klinke, J. B. Hannon, L. Gignac, K. Reuter, and P. Avouris, J. Phys. Chem. B, 109 (2005) 17787.

[32] K. Hong, M. Xie, and H. Wu, Nanotechnology, 17 (2006) 4830.

[33] Y. Baek and K. Yong, J. Phys. Chem. C, 111 (2007) 1213.

[34] Y. Kojima, K. Kasuya, K. Nagato, T. Hamaguchi, and M. Nakao, J. Vac. Sci. Technol. B, 26 (2008) 1942.

[35] J. H. Ha, P. Muralidharana, and D. K. Kim, J. of Alloys and Compounds, 475 (2009) 446.

[36] H. Zhang, T. T. Xu, M. Tang, T. H. Her, and S. Y. Li, J. vac. Sci. Technol. B, 28 (2010) 310.

[37] B. R. Huang, J. C. Lin, T. C. Lin, D. Mangindaan, and M. J. Wang, J. Nanosci. Nanotechnol., 11 (2011) 7693.

Chapter 2

[1] H. Chhina, S. Campbell, and O. Kesler, J. Electrochem. Soc., 154 (2007) B533.

71

[2]   A. Ponzonia, V. Russo, A. Bailini, C. S. Casari, M. Ferroni, A. Li Bassi, A. Migliori, V. Morandi, L. Ortolani, G. Sberveglieri, and C. E. Bottani, Sens. Actuators B, 153 (2011) 340.

[3]   J. Zhou, L. Gong, S. Z. Deng, J. Chen, J. C. She, and N. S. Xu, Applied Physics Letters, 87 (2005) 223108(1).

[4]   P. R. Somani and S. RRadhakrishnan, Chemistry and Physics, 77 (2002) 117.

[5]   S. Balaji, Y. Djaoued, A. S. Albert, R. Z. Ferguson, and R. Bruning, Chem. Mater., 21 (2009) 1381.

[6]   M. Z. Najdoski and T. Todorovski., Materials Chemistry and Physics, 104 (2007) 483.

[7]   C. G. Granqvist, Handbook of Inorganic Electrochromic Materials. 1995, New York: Elsevier.

[8]   C. G. Granqvist, Sol. Energy Mater. Sol. Cells, 60 (2000) 201.

[9]   A. Souza-Filho, V. Freire, J. Sasaki, J. Mendes-Filho, J. Juliao, and U. Gomes, J. Raman Spect., 31 (2000) 451.

[10]   Z. Xu, J. F. Vetelino, R. Lec, and D. C. Parker, J. Vac. Sci. Technol. A, 8 (1990) 3634.

[11]   H. Bouas-Laurent and H. Durr, Pure Appl. Chem., 73 (2001) 639.

[12]   P. M. S. Monk, S. P. Akhtar, J. Boutevin, and J. R. Duffield, , Electrochimica Acta, 46 (2001) 2091.

[13]   G. A. Niklasson, L. Berggren, A. Jonsson, R. Ahuja, N. V. Skorodumova, J. Backholm, and M. Strømme, Solar Energy Materials & Solar Cells, 90 (2006) 385.

[14]   N. A. O'brien, J. Gordon, H. Mathew, and B. P. Hichwa, Thin solid films, 345 (1999) 312.

[15]   P. M. S. Monk, R. J. Mortimer, and D. R. Rosseinsky, Electrochromism and Electrochromic Devices. 2007, United Kingdom: Cambridge University Press.

[16]   Wang, J., Analytical electrochemistry, ed. 3rd. 2006, New York: Wiley.

[17]   C. G. Granqvist, Sol. Energy Mater. Sol. Cells., 92 (2008) 203.

[18]   C. G. Granqvist, A. Azens, A. L. Kullman, G. A. Niklasson, D. Ronnow, M. S. Mattsson, M. Veszelei, and G. Vaivars, Solar Energy, 63 (1998) 199.

[19]   K. Bange, Sol. Energy Mater. Sol. Cells., 58 (1999) 1.

Chapter 3

[1]   S. Jeon and K. Yong, J. Mater. Res. 23 (2008) 1320.

[2]   G. Cao and Y. Wang, Nanostructures and nanomaterials: synthesis, properties, and application. Imperial College Press, 2004.

[3]   B. D. Cullity, Elements of X-Ray Diffraction. Addison-Wesley Pub. Co, 1956.

[4]   J. I. Goldstein, D. E. Newbury, P. Echlin, D. C. Joy, A. D. Romig, C. E. Lyman, C. Fiori, and E. Lifshin, Scanning Electron Microscopy and X-ray Microanalysis. 3th ed. Plenum Press, 2003.

[5]   P. M. S. Monk, R. J. Mortimer, and D. R. Rosseinsky, Electrochromism and Electrochromic Devices. United Kingdom: Cambridge University Press, 2007.

[6]   A. W. Bott and W. R. Heineman, Current Separations. 20 (2004) 121.

Chapter 4

[1]   G. S. Chen, L. C. Yang, H. S. Tian, C. S. Hsu, Thin Solid Films 484 (2005) 83.

[2]   W. Wua, Q. Yua, J. Lianc, J. Baob, Z. Liub and S. S. Pei, J. Crystal Growth 312 (2010) 3147.

[3]   A. H. Jayatissa, S. T. Cheng, T. Gupta, Mater. Sci. Eng. B 109 (2004) 269.

[4]   S. C. Moulzolf, L. J. LeGore, R. J. Lad, Thin Solid Films 400 (2001) 56.

[5]   M. Deepa, A. K. Srivastava , and S. A. Agnihotry, Acta Materialia 54 (2006) 4583.

[6]   M. Ohring, Material Science of Thin Films: Deposition and Structure, Academic Press, USA 2002.

[7]   M. J. Alam and D. C. Cameron, Thin solid films 420-421 (2002) 76.

[8]   M. Deepa, R. Sharma, A. Basu, and S.A. Agnihotry, Electrochim Acta 50 (2005) 3545.

[9]   Wang J, Analytical electrochemistry, 3rd edn. New York: Wiley, 2006.

[10]   B. Gavanier, N. S. Butt, M. Hutchins, V. Mercier, A. J. Topping and J. R. Owen, Electrochim. Acta 44 (1999) 3251.

[11]   C. Brigouleix, P. Toparta, E. Brunetona, F. Sabarya, G. Nouhauta and G. Campet, Electrochim. Acta 46 (2001) 1931.

[12]   Y. Zhang, J. Yuan, J. Le, L. Song, and X. Hu, Sol. Energy Mater. Sol. Cells., 93 (2009) 1338.

Chapter 5

[1]   G. S. Chen, L. C. Yang, H. S. Tian, and C. S. Hsu, Thin solid films, 484 (2005) 83.

[2]   A. H. Jayatissa, S. T. Cheng, and T. Gupta, Mater. Sci. Eng. B, 109 (2004) 269.

[3]   S. Jeon and K. Yong, J. Mater. Res., 23 (2008) 1320.

74

[4]   M. Ohring, Material Science of Thin Films: Deposition and Structure. USA: Academic Press, 2002.

[5]   S. C. Moulzolf, L. J. LeGore, R. J. Lad, Thin Solid Films 400 (2001) 56.

[6]   C. G. Granqvist, Handbook of Inorganic Electrochromic Materials. 1995, New York: Elsevier.

[7]   C. C. Liao, F. R. Chen, J. J. Kai, Sol. Energy Mater. Sol. Cells, 91 (2007) 1258.

[8]   M. J. Alam and D. C. Cameron, Thin solid films, 420-421 (2002) 76.

[9]   M. Deepa, R. Sharma, A. Basu, and S. A. Agnihotry, Electrochimica Acta, 50 (2005) 3545.

[10]   J. Wang, Analytical electrochemistry. New York: Wiley, 2006.

[11]   S. J. Yoo, J. W. Lim, Y. E. Sung, Y. H. Jung, H. G. Choi, and D. K. Kim, Applied Physics Letters, 90 (2007) 173126 (1).

[12]   O. Bohnke, M. Rezrazi, B. Vuillemin, C. Bohnke, P.A. Gillet, and C. Rousselot, Solar Energy Materials and Solar Cell, 25 (1992) 361.

[13]   P. M. S. Monk, R. J. Mortimer, and D. R. Rosseinsky, Electrochromism and Electrochromic Devices. 2007, United Kingdom: Cambridge University Press.

[14]   B. Gavanier, N. S. Butt, M. Hutchins, V. Mercier, A. J. Topping, and J. R. Owen, Electrochimica Acta, 44 (1999) 3251.

[15]   C. Brigouleix, P. Toparta, E. Brunetona, F. Sabarya, G. Nouhauta, and G. Campet, Electrochimica Acta, 46 (2001) 1931.

[16]   H. S. Shim, J. W. Kim, Y. E. Sung, and W. B. Kim, Sol. Energy Mater. Sol. Cells., 93 (2009) 2062.